

# **Global-scale distribution of ozone in the remote troposphere from ATom and HIPPO airborne field missions.**

Ilann Bourgeois<sup>1,2</sup>, Jeff Peischl<sup>1,2</sup>, Chelsea R. Thompson<sup>1,2</sup>, Kenneth C. Aikin<sup>1,2</sup>, Teresa Campos<sup>3</sup>, Hannah Clark<sup>4</sup>, Róisín Commane<sup>5</sup>, Bruce Daube<sup>6</sup>, Glenn W. Diskin<sup>7</sup>, James W. Elkins<sup>8</sup>, Ru-Shan Gao<sup>2</sup>, Audrey Gaudel<sup>1,2</sup>, Eric J. Hintsa<sup>1,8</sup>, Bryan J. Johnson<sup>8</sup>, Rigel Kivi<sup>9</sup>, Kathryn McKain<sup>1,8</sup>, Fred L. Moore<sup>1,8</sup>, David D. Parrish<sup>1,2</sup>, Richard Querel<sup>10</sup>, Eric Ray<sup>1,2</sup>, Ricardo Sánchez<sup>11</sup>, Colm Sweeney<sup>7</sup>, David W. Tarasick<sup>12</sup>, Anne M. Thompson<sup>13</sup>, Valérie Thouret<sup>14</sup>, Jacquelyn C. Witte<sup>3</sup>, Steve C. Wofsy<sup>6</sup>, and Thomas B. Ryerson<sup>2</sup>.

<sup>1</sup>Cooperative Institute for Research in Environmental Sciences, University of Colorado Boulder, Boulder, CO, USA

<sup>2</sup>NOAA CSL, Boulder, CO, USA

<sup>3</sup>National Center for Atmospheric Research, Boulder, CO, USA

<sup>4</sup>IAGOS-AISBL, Brussels, Belgium

<sup>5</sup>Department of Earth and Environmental Sciences, Lamont-Doherty Earth Observatory of Columbia University, New York, NY, USA

<sup>6</sup>School of Engineering and Applied Sciences, Harvard University, Cambridge, MA, USA

<sup>7</sup>NASA Langley Research Center, Hampton, VA, USA

<sup>8</sup>NOAA GML, Boulder, CO, USA

<sup>9</sup>Finnish Meteorological Institute, Space and Earth Observation Centre, Sodankylä, Finland

<sup>10</sup>National Institute of Water & Atmospheric Research (NIWA), Lauder, NZ

<sup>11</sup>Servicio Meteorológico Nacional, Buenos Aires, Argentina

<sup>12</sup>Experimental Studies Research Division, MSC/Environment and Climate Change Canada, Downsview, Ontario, CA

<sup>13</sup>Earth Sciences Division, NASA/Goddard Space Flight Center, Greenbelt, MD, USA

<sup>14</sup>Laboratoire d'Aérodynamique, CNRS and Université Paul Sabatier, Université de Toulouse, Toulouse, FR

## Abstract

Ozone is a key constituent of the troposphere where it drives photochemical processes, impacts air quality, and acts as a climate forcer. Large-scale in situ observations of ozone commensurate with the grid resolution of current Earth system models are necessary to validate model outputs and satellite retrievals. In this paper, we examine measurements from the Atmospheric Tomography (ATom, 4 deployments in 2016–2018) and the HIAPER Pole-to-Pole Observations (HIPPO; 5 deployments in 2009–2011) experiments, two global-scale airborne campaigns covering the Pacific (HIPPO and ATom) and Atlantic (ATom) basins.

ATom and HIPPO represent the first global-scale, vertically resolved measurements of O<sub>3</sub> distributions throughout the troposphere, with HIPPO sampling the Pacific basin and ATom sampling both the Pacific and Atlantic basins. Given the relatively limited temporal resolution of these two campaigns, we first compare ATom and HIPPO ozone data to longer-term observational records to establish the representativeness of our dataset. We show that these two airborne campaigns captured on average 53, 54, and 38 % of the ozone variability in the marine boundary layer, free troposphere, and upper troposphere/lower stratosphere (UTLS), respectively, at nine well-established ozonesonde sites. Additionally, ATom captured the most frequent ozone concentrations measured by regular commercial aircraft flights in the northern Atlantic UTLS. We then use the repeated vertical profiles carried out during these two campaigns to **confirm and extend the existing knowledge global-scale picture** of tropospheric ozone spatial and vertical distributions throughout the remote troposphere. We highlight a clear hemispheric gradient, with greater ozone in the northern hemisphere consistent with greater precursor emissions, **on par with previous modeling and satellite studies**. We also show that the ozone distribution below 8 km was similar in the extra-tropics of the Atlantic and Pacific basins **likely** due to zonal circulation patterns. However, twice as much ozone was found in the tropical Atlantic than in the tropical Pacific, due to well-documented dynamical patterns transporting continental air masses over the Atlantic. **Finally, we** show that the seasonal variability of tropospheric ozone over the Pacific and the Atlantic basins is driven by transported continental plumes and photochemistry, and the vertical distribution is driven by photochemistry and mixing with stratospheric air. This new dataset **provides additional constraints for global climate and chemistry models to improve our** understanding of both ozone production and loss processes in remote regions, as well as the influence of anthropogenic emissions on baseline ozone.

## 1. Introduction

Tropospheric ozone ( $O_3$ ) plays a major role in local, regional, and global air quality and significantly influences Earth's radiative budget (IPCC, 2013; Shindell et al., 2012). In addition,  $O_3$  drives tropospheric photochemical processes by controlling hydroxyl radical (OH) abundance, which subsequently controls the lifetime of other pollutants including volatile organic compounds (VOCs), greenhouse gases, and some stratospheric ozone-depleting substances (Crutzen, 1974; Levy, 1971). Sources of  $O_3$  to the troposphere include downward transport from the stratosphere (Junge, 1962) and photochemical production from precursors such as carbon monoxide (CO), methane ( $CH_4$ ), and VOCs in the presence of nitrogen oxides ( $NO_x$ ) emitted by natural or anthropogenic sources (Monks et al., 2009). Tropospheric  $O_3$  sinks include photo-dissociation, chemical reactions, and dry deposition. Owing to its relatively long lifetime ( $\sim 23$  days in the troposphere; Young et al., 2013),  $O_3$  can be transported across intra-hemispheric scales.  $O_3$  mixing ratios over a region thus depend not only on local and regional sources and sinks, but also on long-range transport. Further, the uneven density of  $O_3$  monitoring locations around the globe leads to significant sampling gaps, especially near developing nations (Gaudel et al., 2018). The troposphere over the remote oceans is among the least-sampled regions, despite hosting 60–70 % of global tropospheric  $O_3$  burden (Holmes et al., 2013).

Since the early 1980's, several aircraft campaigns have periodically addressed this paucity of remote observations, most notably under the umbrella of the Global Tropospheric Experiment (GTE), a major component of the National Aeronautics and Space Administration (NASA) Tropospheric Chemistry Program ([https://eosweb.larc.nasa.gov/project/gte/gte\\_table](https://eosweb.larc.nasa.gov/project/gte/gte_table)). Airborne campaigns have targeted both the Pacific and Atlantic Oceans, providing novel characterization of  $O_3$  sources, distribution, and photochemistry in the marine troposphere (Browell et al., 1996a; Davis et al., 1996; Jacob et al., 1996; Pan et al., 2015; Schultz et al., 1999; Singh et al., 1996c) and the low- $O_3$  tropical Pacific pool (Kley et al., 1996; Singh et al., 1996b), the pervasive role of continental outflow on  $O_3$  production (Bey et al., 2001; Crawford et al., 1997; Heald et al., 2003; Kondo et al., 2004; Martin et al., 2002; Zhang et al., 2008), and the marked influence of African and South American biomass burning on  $O_3$  production in the Southern Hemisphere (Browell et al., 1996b; Fenn et al., 1999; Mauzerall et al., 1998; Singh et al., 1996a; Thompson et al., 1996). Ozonesondes have been launched from remote sites for more than three decades in some places, and have provided additional constraints on the sources and

photochemical balance of tropospheric O<sub>3</sub> including a deep understanding of vertically-resolved tropospheric O<sub>3</sub> climatology in select locations (Derwent et al., 2016; Diab et al., 2004; Jensen et al., 2012; Liu et al., 2013; Logan, 1985; Logan and Kirchhoff, 1986; Newton et al., 2017; Oltmans et al., 2001; Parrish et al., 2016; Sauvage et al., 2006; Thompson et al., 2012). Spatially-resolved O<sub>3</sub> climatology has been provided by routine sampling by commercial aircraft, but has mostly been limited to the upper troposphere or over continental regions (Clark et al., 2015; Cohen et al., 2018; Logan et al., 2012; Petetin et al., 2016; Sauvage et al., 2006; Thouret et al., 1998; Zbinden et al., 2013), and by satellite observations (Edwards et al., 2003; Fishman et al., 1990, 1991; Hu et al., 2017; Thompson et al., 2017; Wespes et al., 2017; Ziemke et al., 2005, 2006, 2017), somewhat tempered by large uncertainties (Tarasick et al., 2019a). Recent overview analyses depict the current understanding of global tropospheric O<sub>3</sub> sources, distribution, and photochemical balance and underscore the insufficiency of observations in the remote free troposphere (Cooper et al., 2014; Gaudel et al., 2018; Tarasick et al., 2019a) necessary to improve the current representation of tropospheric O<sub>3</sub> in global chemical models (Young et al., 2018). Spatial and temporal representativeness of O<sub>3</sub> observations is currently the biggest source of uncertainty when inferring O<sub>3</sub> climatology in the free troposphere, even in regions where observation are abundant but not ideally distributed (Lin et al., 2015a; Tarasick et al., 2019a).

The Atmospheric Tomography mission (ATom, <https://espo.nasa.gov/atom>) was a NASA Earth Venture airborne field project to address the sparseness of atmospheric observations over remote ocean regions by systematically sampling the troposphere over the Pacific and Atlantic basins along a global-scale circuit (Fig. 1). ATom deployed an extensive payload on the NASA DC-8 aircraft, measuring a wide range of chemical, microphysical, and meteorological parameters in repeated vertical profiles from 0.2 km to over 13 km altitude, from the Arctic to the Antarctic over the Pacific and Atlantic Oceans, in four separate seasons from 2016 to 2018. One of the main goals of ATom was to develop an observation-based climatology of the composition of the remote atmosphere using airborne in situ measurements from global-scale sampling flights. ATom built on a previous study, the HIAPER Pole-to-Pole Observations mission (HIPPO, [https://www.eol.ucar.edu/field\\_projects/hippo](https://www.eol.ucar.edu/field_projects/hippo)). The goal of HIPPO was to measure atmospheric distributions of important greenhouse gases and reactive species over the Pacific Ocean, from the surface to the tropopause, five times during different seasons from 2009 to 2011. Together, ATom and HIPPO provide recent and comprehensive information about the

altitudinal, latitudinal, and seasonal composition of the remote troposphere over the Pacific, and over the Atlantic for ATom. In addition, ATom and HIPPO sampling strategies were designed to deliver an objective climatology of key species to enable modelling of air parcel reactivity of the remote troposphere (Prather et al., 2017).

Here we use existing ozonesonde and commercial aircraft observations of O<sub>3</sub> at selected locations along the ATom and HIPPO circuits to provide a climatological context for the altitudinal, latitudinal, and seasonal distributions of O<sub>3</sub> derived from the systematic airborne in situ “snapshots”. Long-term O<sub>3</sub> observations are obtained from decades of ozonesonde vertical profiles (e.g., Oltmans et al., 2013; Thompson et al., 2017) and from ~60,000 flights using the In-service Aircraft for a Global Observing System (IAGOS) infrastructure (Petzold et al., 2015; <http://www.iagos.org>). Ozonesondes have typically been launched weekly for two decades or more, depending on the site, and have sampled a wide range of air masses across the globe, from O<sub>3</sub>-poor remote surface locations to the O<sub>3</sub>-rich stratosphere. IAGOS commercial aircraft have provided daily measurements in the upper troposphere and lower stratosphere (UTLS) for the past 25 years, especially over the northern midlatitudes between America and Europe. Combined, the ozonesonde and IAGOS datasets offer robust measurement-based climatologies that quantify the full expected range of atmospheric O<sub>3</sub> variability with altitude and season. The in-situ data from temporally-limited intensive field studies can be placed in context by comparing them with long-term ozonesonde and commercial aircraft monitoring data. We show that ATom and HIPPO measurements capture the spatial and, in some cases, the temporal dependence of O<sub>3</sub> in the remote atmosphere. Then, we use the geographically extensive ATom and HIPPO vertical profile data to establish a more complete measurement-based benchmark for O<sub>3</sub> abundance and distribution in the remote marine atmosphere.

## 2. Measurements

### 2.1 ATom

The four ATom circuits occurred in July–August 2016 (ATom-1), January–February 2017 (ATom-2), September–October 2017 (ATom-3), and April–May 2018 (ATom-4), thus spanning all four seasons in both hemispheres over a two-year timeframe (Table S1). The mission in total consisted of 48 science flights and 548 vertical profiles distributed nearly equally along the global circuit. All four deployments completed roughly the same loop, starting and

ending in Palmdale, California, USA (Fig. 1). A notable addition during ATom-3 and -4 were out-and-back flights from Punta Arenas, Chile to sample the Antarctic troposphere and UTLS.

O<sub>3</sub> was measured using the National Oceanic and Atmospheric Administration (NOAA) nitrogen oxides and ozone (NO<sub>y</sub>O<sub>3</sub>) instrument. The O<sub>3</sub> channel of the NO<sub>y</sub>O<sub>3</sub> instrument is based on the gas-phase chemiluminescence (CL) detection of ambient O<sub>3</sub> with pure NO added as a reagent gas (Ridley et al., 1992; Stedman et al., 1972). Ambient air is continuously sampled from a pressure-building ducted aircraft inlet into the NO<sub>y</sub>O<sub>3</sub> instrument at a typical flow rate of  $1025.0 \pm 0.2$  standard cubic centimeters per minute (sccm) in flight. Pure NO reagent gas flow delivered at  $3.450 \pm 0.006$  sccm is mixed with sampled air in a pressure ( $8.00 \pm 0.08$  Torr) and temperature ( $24.96 \pm 0.01$  °C) controlled reaction vessel. NO-induced CL is detected with a dry-ice-cooled, red-sensitive photomultiplier tube and the amplified digitized signal recorded using an 80 MHz counter; pulse coincidence corrections at high count rates were applied, but are negligible for the data presented in this work. The instrument sensitivity for measuring O<sub>3</sub> under these conditions is  $3150 \pm 80$  counts per second per part per billion by volume (ppbv) averaged over the entire ATom circuit. CL detector calibrations were routinely performed both on the ground and during flight by standard addition of O<sub>3</sub> produced by irradiating ultrapure air with 185 nm UV light and independently measured using UV optical absorption at 254 nm. All O<sub>3</sub> measurements were taken at a temporal resolution of 10 Hz, averaged to 1 Hz, and corrected for the dependence of instrument sensitivity on ambient water vapor content (Ridley et al., 1992). Under these conditions the total estimated 1 Hz uncertainty at sea level is  $\pm (0.015 \text{ ppbv} + 2 \%)$ .

A commercial dual-beam photometer (2B Technologies model 211) based on UV optical absorption at 254 nm also measured O<sub>3</sub> on ATom, with an estimated uncertainty of  $\pm (1.5 \text{ ppbv} + 1 \%)$  at a 2-second sampling resolution. Comparison of the 2B absorption instrument O<sub>3</sub> data to the NO<sub>y</sub>O<sub>3</sub> CL instrument O<sub>3</sub> data agreed to within combined instrumental uncertainties, lending additional confidence to the NO<sub>y</sub>O<sub>3</sub> CL instrument calibration. For the ATom project we use NO<sub>y</sub>O<sub>3</sub> instrument O<sub>3</sub> data in the following analyses.

Data from two CO measurements were combined in this analysis. The Harvard quantum cascade laser spectrometer (QCLS) instrument used a pulsed quantum cascade laser tuned at  $\sim 2160 \text{ cm}^{-1}$  to measure the absorption of CO through an astigmatic multi-pass sample cell with 76 m path length and detection using a liquid-nitrogen-cooled HgCdTe detector (Santoni et al., 2014). In-flight calibrations were conducted with gases traceable to the NOAA World

Meteorological Organization (WMO) X2014A scale, and the QCLS observations have an accuracy and precision of 3.5 and 0.15 ppb for 1 Hz data, respectively. CO was also measured by the NOAA cavity ring-down spectrometer (CRDS, Picarro, Inc., model G2401-m) in the 1.57  $\mu\text{m}$  region with a total uncertainty of 5.0 ppbv for 1 Hz data (Karion et al., 2013). The NOAA Picarro was also calibrated to the NOAA CO-X2014A scale. The combined CO data (CO-X) used here corresponds to the QCLS data, with the Picarro measurement used to fill calibration gaps in the QCLS time series.

Water ( $\text{H}_2\text{O}$ ) vapor was measured using the NASA Langley Diode Laser Hygrometer (DLH), an open-path infrared absorption spectrometer that uses a laser locked to a water vapor absorption feature at  $\sim 1.395 \mu\text{m}$ . Raw data are processed at the instrument's native  $\sim 100$  Hz acquisition rate and averaged to 1 Hz with an overall measurement accuracy within 5 %.

## 2.2 HIPPO

The HIPPO mission consisted of five seasonal deployments over the Pacific basin between 2009 and 2011, from the North Pole to the coastal waters of Antarctica (Wofsy, 2011). HIPPO deployments consisted of two transects, southbound and northbound, and occurred in January 2009 (HIPPO-1), October–November 2009 (HIPPO-2), March–April 2010 (HIPPO-3), June–July 2011 (HIPPO-4) and August–September 2011 (HIPPO-5). The platform used was the NSF Gulfstream V (GV) aircraft. More details can be found in Table S1.

A NOAA custom-built dual-beam photometer based on UV optical absorption at 254 nm was used to measure  $\text{O}_3$  (Proffitt and McLaughlin, 1983). The uncertainty of the 1 Hz  $\text{O}_3$  data is estimated to be  $\pm (1 \text{ ppbv} + 5 \%)$  for 1 Hz data. A commercial dual-beam  $\text{O}_3$  photometer (2B Technologies model 205) based on UV optical absorption at 254 nm was also included in the HIPPO payload. Comparison of the 2B  $\text{O}_3$  data to the NOAA  $\text{O}_3$  data showed general agreement within combined instrument uncertainties on level flight legs. For the HIPPO project we use NOAA  $\text{O}_3$  data in the following analyses.

Data from two CO measurements were combined in this analysis. The QCLS instrument was the same instrument as used during ATom and described in section 2.1. CO was also measured by an Aero-Laser AL5002 instrument using vacuum UV resonance fluorescence (in the 170–200 nm range) instrument with an uncertainty of  $\pm (2 \text{ ppbv} + 3 \%)$  at a 2-second

sampling resolution. The combined CO data (CO-X) used here corresponds to the QCLS data, with the Aero-Laser measurement used to fill calibration gaps in the QCLS time series.

## 2.3 IAGOS

IAGOS is a European Research Infrastructure that provides airborne in situ chemical, aerosol, and meteorological measurements using commercial aircraft (Petzold et al., 2015). The IAGOS Research Infrastructure includes data from both the CARIBIC (Civil Aircraft for the Regular Investigation of the atmosphere Based on an Instrument Container; Brenninkmeijer et al., 2007) and MOZAIC (Measurements of OZone and water vapor by Airbus In-service airCRAFT; Marenco et al., 1998) programs, providing measurements from ~60,000 flights since 1994. We note the relative lack of IAGOS data over the Pacific compared to the Atlantic (shorter temporal record, lower flight frequency, and much fewer flights with concomitant O<sub>3</sub> and CO measurements), and therefore limited the comparison to the Atlantic. Because commercial aircraft cruise altitudes over the ocean are predominantly between 9 and 12 km, the comparison between ATom and IAGOS is further limited to the UTLS (Fig. 1). More details are shown in Table S1.

Identical dual-beam UV absorption photometers measured O<sub>3</sub> aboard the IAGOS flights. An instrument comparison demonstrated that the photometers (standard model 49, Thermo Scientific, modified for aircraft use) showed good consistency in measuring O<sub>3</sub> following an inter-comparison experiment (Nédélec et al., 2015). The associated uncertainty is  $\pm (2 \text{ ppbv} + 2 \%)$  at a 4-second sampling resolution (Thouret et al., 1998).

CO measurements were made using infra-red absorption photometers (standard model 48 Trace Level, Thermo Scientific, modified for aircraft use) with an uncertainty of  $\pm (5 \text{ ppbv} + 5 \%)$  at a 30-second sampling resolution (Nédélec et al., 2003, 2015).

## 2.4 Ozonesondes

Ozonesondes have measured the vertical distribution of O<sub>3</sub> in the atmosphere for decades, and provide some of the longest tropospheric records that are commonly used to determine regional O<sub>3</sub> trends (Gaudel et al., 2018; Leonard et al., 2017; Oltmans et al., 2001; Tarasick et al., 2019a; Thompson et al., 2017). Ozonesonde launching sites are operated by the NOAA ESRL Global Monitoring Division (GMD), NASA Goddard's Southern Hemisphere Additional



OZonesondes (SHADOZ) program, the New Zealand National Institute of Water & Atmospheric Research (NIWA), the National Meteorological Center of Argentina (SNMA) in collaboration with the Finnish Meteorological Institute (FMI), or Environment and Climate Change Canada. A more detailed description of each ozonesonde site and corresponding dataset can be found in Tables S1 and S2. All sites use electrochemical concentration cell (ECC) ozonesondes that rely on the potassium iodide electrochemical detection of O<sub>3</sub>, and which provide a vertical resolution of about 100 m (Komhyr, 1969). The associated uncertainty is usually  $\pm$  (5–10 %) (Tarasick et al., 2019a; Thompson et al., 2019; Witte et al., 2018).

## 2.5 Data analysis

In this analysis, ATom flight tracks were divided into the Atlantic and Pacific basins, and further subdivided into five regions within those basins: tropics, and northern and southern middle- and high-latitudes. Vertical profiles presented graphically in this paper show O<sub>3</sub> median values and the 25<sup>th</sup> to 75<sup>th</sup> percentile range within the 0–12 km tropospheric column sampled by the DC-8 aircraft. These medians were obtained by averaging with equal weight the individual profiles within each region over 1 km altitude bins.

HIPPO flight tracks are illustrated in Figure 1. The flight segments used for comparison with ATom were binned into the same Pacific latitude and longitude bands as for ATom. HIPPO vertical profile data are derived using the same methodology as for ATom.

All IAGOS flight tracks over the northern and tropical Atlantic are represented in Figure 1 in green. The latitude bands used to parse IAGOS data are consistent with the ones used for ATom. The longitude bands are 50° W to 20° W in the tropics, 50° W to 10° W in the northern midlatitudes, and 110° W to 10° W in the northern high-latitudes. Variations of the longitude band widths do not significantly affect the O<sub>3</sub> distributions measured by IAGOS. Data from all flights from 1994 to 2017 were included in the IAGOS dataset considered here, and were then divided into two altitude bins (8–10 km and 10–12 km) in order to better understand the influence of different O<sub>3</sub> sources (e.g., anthropogenic, stratospheric) on these two layers of the atmosphere.

We compare the ozonesonde measurements to ATom and HIPPO aircraft data sampled within 500 km of each ozonesonde launching site, since we expect a robust correlation in the free troposphere within this distance (Liu et al., 2009). We used the surface coordinates of the

ozonesonde sites because the in-flight coordinates of ozonesondes are not available at all sites. For comparison with ozonesonde long term records, we consider three regions of the atmosphere: boundary layer (0–2 km), free troposphere (2–8 km), and UTLS (8–12 km). For each layer, we compared monthly O<sub>3</sub> distributions from ozonesondes with the corresponding seasonal O<sub>3</sub> distributions from aircraft measurements using the skill score ( $S_{score}$ ) metric (Perkins et al., 2007). The  $S_{score}$  is calculated by summing the minimum probability of two normalized distributions at each bin center, and therefore measures the overlapping area between two probability distribution functions. If the distributions are identical, the skill score will equal 100 % (see Fig. S1 for further examples). Note the  $S_{score}$  is positively correlated with the size of the bin used to compare distributions. Here we chose a bin size of 5 ppbv, which is larger than the combined precision of ATom, HIPPO, and IAGOS measurements, but small enough to separate distinct air masses and their influence on O<sub>3</sub> distribution. Variables such as the distance to each ozonesonde launching site (500 km in this study), the bin size of the O<sub>3</sub> distributions (5 ppbv in this study), and the length of each ozonesonde record (full length in this study) can shift the vertically-averaged  $S_{score}$  value by up to 8 % (Table S3). We therefore treat this 8 % as a rough estimate of the precision of the  $S_{score}$  values presented here.

All three techniques (chemiluminescence, UV absorption, and ECC) used to measure O<sub>3</sub> for the datasets analyzed in this work have been shown to provide directly-comparable accurate measurements with well-defined uncertainties (Tarasick et al., 2019a).

## 2.6 Back trajectory analysis

Analysis of back trajectories for air masses sampled during airborne missions is useful to examine the air mass source regions and causes for O<sub>3</sub> variability over the Pacific and Atlantic Oceans. We calculated ten-day back trajectories using the Traj3D model (Bowman, 1993; Bowman and Carrie, 2002) and National Centers for Environmental Prediction (NCEP) global forecast system (GFS) meteorology. Trajectories were initialized each minute along all of the ATom flight tracks.

## 3. **Comparison of ATom and HIPPO O<sub>3</sub> distributions to longer-term observational records**

Here we use existing ozonesonde and IAGOS observations of O<sub>3</sub> at selected locations along the ATom and HIPPO circuits to provide a climatological context for O<sub>3</sub> distributions derived from the systematic airborne in situ “snapshots”. We quantify how much of O<sub>3</sub> variability, occurring on timescales ranging from hours to decades, was captured by the temporally-limited HIPPO and ATom missions.

### 3.1. Comparison to ozonesondes

ATom and HIPPO explored the fidelity with which airborne missions represent O<sub>3</sub> climatology in the remote troposphere. Here, we show that aircraft-measured median O<sub>3</sub> follows the seasonal ozonesonde-measured median O<sub>3</sub> cycle at most of the sites studied here, and at almost all altitudes – with a few exceptions (Figs. 2 and 3). Figure 2 plots the monthly median O<sub>3</sub> measurements from the tropical ozonesonde sites in three altitude bins, along with the median values obtained from HIPPO and ATom measurements. Figure 3 plots the same for the extratropical sites. Figure 4 correlates the median O<sub>3</sub> measured by aircraft in Figures 2 and 3 with those measured by ozonesondes. At the Eureka site, the winter and spring ATom deployments recorded a significantly lower median O<sub>3</sub> compared to the corresponding ozonesonde monthly median O<sub>3</sub> in the 0–2 km range (Fig. 3). Eureka is frequently subject to springtime O<sub>3</sub> depletion events at the surface due to atmospheric bromine chemistry, which is well recorded by the ozonesonde record (Fig. 3; Tarasick and Bottenheim, 2002). Sampling during O<sub>3</sub> depletion events significantly lowered the ATom winter and springtime O<sub>3</sub> distributions near this site. In the 2–8 km range, there is a very good seasonal agreement between ATom/HIPPO and the ozonesondes (Fig. 4b). Most seasonal differences are found above 8 km (e.g., ATom in February at Trinidad Head and in May at Eureka; Fig. 3) and can be linked to the occurrence – or absence – of stratospheric air sampling during ATom and HIPPO. However, it is straightforward to remove stratospheric airmasses from airborne data using filters based on meteorology (potential vorticity) or composition (H<sub>2</sub>O/O<sub>3</sub>) (e.g., Cohen et al., 2018). In the absence of stratospheric air mixing (< 8 km in Fig. 4), ATom/HIPPO successfully capture a large fraction of O<sub>3</sub> climatology everywhere (Figs. 4b and 4c).

Figures 5 and 6 show vertical profiles of O<sub>3</sub> distributions by season at each ozonesonde site, along with comparisons to HIPPO and ATom vertical profiles. Our analysis reveals that O<sub>3</sub>

distributions derived from the ATom and HIPPO seasonal “snapshots” capture 30–71 % of the 1 km-vertically binned O<sub>3</sub> distribution established by long-term ozonesonde climatologies. For the nine ozonesonde sites considered here, ATom and HIPPO captured on average 53 %, 54 %, and 38 % of the O<sub>3</sub> distribution in the 0–2 km, 2–8 km, and 8–12 km altitude bins, respectively.

Larger differences between ATom/HIPPO and the ozonesonde records in the UTLS (8–12 km) can be ascribed to O<sub>3</sub> variability from stratospheric–tropospheric exchanges, which are not always captured by the ATom and HIPPO missions. This increased O<sub>3</sub> variability in the UTLS is well-described by the long term ozonesonde records at Lauder, Trinidad Head, Eureka, Ushuaia, and Marambio (Figs. 3 and 6). In these middle- and high-latitude locations in both hemispheres, O<sub>3</sub> variability is especially pronounced during winter and spring, time periods favorable to more frequent stratospheric air mixing (Greenslade et al., 2017; Lin et al., 2015b; Tarasick et al., 2019b). Furthermore, the probability of sampling stratospheric air masses at ATom and HIPPO ceiling altitude (12–14 km) increases with latitude, resulting in a lower  $S_{score}$  between the ATom/HIPPO and ozonesonde datasets at the extra-tropical sites than at the tropical sites (Figs. S2a and S2b).

In the boundary layer (0–2 km) of the remote troposphere, O<sub>3</sub> variability is predominantly impacted by loss mechanisms. Ozonesonde records show instances of O<sub>3</sub> mixing ratios lower than 10 ppbv throughout the year in the boundary layer at the nine sites studied here (Figs. 2 and 3). The lowest O<sub>3</sub> mixing ratios are a result of (a) photochemical destruction over the oceans in the tropics (Monks et al., 1998, 2000; Thompson et al., 1993), (b) O<sub>3</sub>-destroying halogen emissions in polar regions in springtime (e.g., Fan and Jacob, 1992), and (c) transport of O<sub>3</sub>-poor oceanic air over the midlatitude sites (e.g., Neuman et al., 2012).

ATom and HIPPO best describe the O<sub>3</sub> distribution in the free troposphere (2–8 km; Figs. S2a and S2b). This suggests that airborne campaigns can capture global baseline O<sub>3</sub> values, along with the long-range transport of O<sub>3</sub> pollution plumes often lofted to this altitude range and responsible for O<sub>3</sub> variability.

While ATom consisted of one transect per ocean per season, HIPPO covered the Pacific twice per seasonal deployment (southbound and northbound). The 1 km-binned  $S_{score}$  is on average higher when two combined seasonal HIPPO flights (southbound and northbound) were available to compare to ozonesonde records, as opposed to when comparing O<sub>3</sub> profiles from

individual HIPPO transects with ozonesonde records (Fig. S2c). In addition, two seasonal flights during HIPPO reduced the occurrence of low  $S_{score}$  values. This  $S_{score}$  decrease from flying only one Pacific transect only during ATom was traded for the increase of vertical profiles over the Atlantic Basin, which were not sampled during HIPPO. Future airborne missions with multiple seasonal vertical profiles over large-scale regions would be ideal to better depict the full range of tropospheric  $O_3$  variability.

### 3.2. Comparison to IAGOS

IAGOS  $O_3$  and CO observations in the northern Atlantic UTLS provide a measurement-based climatology at commercial aircraft cruise altitudes for comparison to ATom. Simultaneous measurements of  $O_3$  and CO are of particular interest because CO provides a long-lived tracer of continental emissions, which helps to differentiate  $O_3$  sources (Cohen et al., 2018). We note that while IAGOS measurements encompass hundreds of seasonal flights (depending on the region), ATom sampled within each latitude band and season on one or two flights only (Fig. 1). Thus, variability in the UT that occurred on timescales longer than a day were not captured by ATom. Consequently, it is not surprising to see that ATom systematically under-sampled tropospheric  $O_3$  (and CO) variability compared to IAGOS at all latitudes in the northern Atlantic (Figs. 7 and 8). ATom captured on average 40 % of the  $O_3$  variability measured by IAGOS in the Atlantic UTLS (Fig. 7), on par with the  $S_{score}$  of 38 % obtained when comparing ATom and HIPPO to ozonesonde data (see section 3.1).

In the middle- and high-latitudes, the shapes of the  $O_3$  vs. CO scatterplots from IAGOS data demonstrate that distinct sources contribute to  $O_3$  levels in the UTLS (Figs. 8a and 8b; Gaudel et al., 2015). The high  $O_3$  (>150 ppbv) – low CO (<100 ppbv) range corresponds to intrusions of stratospheric air, which were mostly sampled in the spring season during ATom, supporting previous observations of increased stratospheric air mixing during this season (Lin et al., 2015b; Tarasick et al., 2019b). The low  $O_3$  (<50 ppbv) – low CO (<100 ppbv) range corresponds to the tropospheric baseline air, whereas the intermediate  $O_3$  (50–120 ppbv) – high CO (>100 ppbv) range generally represents the influence of air masses transported from continental regions. During ATom, high  $O_3$  and low CO in the middle- and high-latitude UTLS were typical of stratospheric and baseline tropospheric air mixing.

O<sub>3</sub> measured during IAGOS rarely exceeds 150 ppbv in the northern tropical Atlantic UTLS (Fig. 8c). This is expected because the tropical tropopause is typically situated between 13 and 17 km altitude and IAGOS flights typically cruise below 12 km. Therefore, instances of stratospheric intrusions at IAGOS flight altitudes are limited. O<sub>3</sub> measured during ATom in the tropical Atlantic above 8 km was generally positively correlated with CO, showing the contribution of tropospheric O<sub>3</sub> production from continental sources reaching high altitudes. Given this variability, the ATom data do not capture the extrema of UTLS O<sub>3</sub> variability in the IAGOS measurements (Figs. 7 and 8). However, the most frequently measured O<sub>3</sub> and CO values from ATom overlap with the most frequently measured O<sub>3</sub> and CO values from IAGOS (contours in Fig. 8), suggesting that ATom captured the mode of the O<sub>3</sub> and CO distributions from IAGOS in the northern Atlantic UTLS.

#### 4. O<sub>3</sub> distributions in the remote troposphere from ATom and HIPPO

We have established the fidelity of ATom and HIPPO O<sub>3</sub> data by comparison to measurement-based climatologies of tropospheric O<sub>3</sub> from well-established ozonesonde and commercial aircraft monitoring programs. In the following sections we exploit the systematic nature of the ATom and HIPPO vertical profiles to provide a global-scale picture of tropospheric O<sub>3</sub> distributions in the remote atmosphere. Figure 9 presents the altitudinal, latitudinal, and seasonal distribution of tropospheric O<sub>3</sub> during ATom and HIPPO. Higher O<sub>3</sub> was measured during ATom & HIPPO in the Northern Hemisphere (NH) than in the Southern Hemisphere (SH), both in the Pacific and in the Atlantic. **This distribution gradient has previously been shown by global O<sub>3</sub> mapping from modeling, satellite, and ozonesonde analyses (e.g., Hu et al., 2017; Liu et al., 2013).** This finding holds true throughout the tropospheric column from 0 to 8 km, both in the middle- and high-latitudes (Fig. S3). In the midlatitudes below 8 km, median O<sub>3</sub> ranged between 25 and 45 ppbv in the SH, and between 35 and 65 ppbv in the NH. In the high latitudes below 8 km, median O<sub>3</sub> ranged between 30 and 45 ppbv in the SH, and between 40 and 75 ppbv in the NH. Notable features in the global O<sub>3</sub> distribution are discussed in more detail in the following sections. Figure 10 presents the vertically-resolved distribution of tropospheric O<sub>3</sub> from 0–12 km for the Atlantic (ATom in green) and for the Pacific (ATom in pink, HIPPO in blue).  $S_{score}$  values resulting from the comparison of HIPPO and ATom Pacific distributions are

shown with blue diamonds, and from the comparison of ATom Atlantic and Pacific distributions with pink squares. Figure 11 is derived from Figure 10 and gives the  $S_{score}$  values against altitude in the first panel, as well as the relative difference of median  $O_3$  from 0 to 8 km in the second panel.

#### 4.1. Tropics

**Vertical distribution.**  $O_3$  is at a minimum in the tropical marine boundary layer (MBL), especially over the Pacific (Fig. 10a). The lowest measured  $O_3$  in this region was 5.4 ppbv in May during ATom, and 3.5 ppbv in January during HIPPO. The tropical MBL is a net  $O_3$  sink owing to very slow  $O_3$  production rates – NO levels averaged  $22 \pm 12$  pptv in the Pacific and Atlantic MBL during ATom – and rapid photochemical destruction rates of  $O_3$  in a sunny, humid environment (Kley et al., 1996; Parrish et al., 2016; Thompson et al., 1993). Deep stratospheric intrusions into the Pacific MBL were not observed in ATom or HIPPO, in contrast to reports from previous studies (e.g., Cooper et al., 2005; Nath et al., 2016). In the tropics, marine convection within the intertropical convergence zone (ITCZ) is associated with relatively low  $O_3$  values throughout the tropospheric column, with median  $O_3$  mixing ratios less than 25 ppbv below 4 km altitude in the tropical Pacific (Fig. 10a; Oltmans et al., 2001). The relative difference between ATom Atlantic and Pacific median  $O_3$  in the tropics below 8 km is consistently higher than a factor of 1.5, with an average  $S_{score}$  of 43 % (Figs. 10a and 11b). We ascribe this difference to  $O_3$  production from biomass burning (BB) emissions in the continental regions surrounding the tropical Atlantic; back trajectories from the ATom flight tracks show the tropical Atlantic is strongly affected by transport from BB source regions in both Africa and South America (Fig. S4; Jensen et al., 2012; Sauvage et al., 2006; Stauffer et al., 2018; Thompson et al., 2000). In addition, the positive correlation of  $O_3$  enhancements with black carbon (Katich et al., 2018) and reactive nitrogen species (Thompson et al., personal communication) also indicate BB influence. Although ATom and HIPPO data show evidence for extensive and widespread BB influence on  $O_3$  in the Pacific as well,  $O_3$  mixing ratios are consistently more elevated throughout the tropospheric column in the Atlantic. One reason is closer proximity of the mid-ocean Atlantic flight tracks to  $O_3$  precursor source regions. These findings confirm studies that previously highlighted the impact of African BB emissions on  $O_3$  production in the tropical Atlantic (e.g., Andreae et al., 1994; Fishman et al., 1996; Jourdain et

al., 2007; Williams et al., 2010). Lightning  $\text{NO}_x$  also play a role in the buildup of  $\text{O}_3$  over the tropical Atlantic at certain times of year (Moxim and Levy, 2000; Pickering et al., 1996).

**Seasonality.** The seasonal variation of vertical profiles of  $\text{O}_3$  in the tropics is lower throughout the column compared to the extra-tropics (Fig. 12), in part due to less stratospheric influence at the highest tropical altitudes. The remoteness of the tropical Pacific flight paths from continental pollution sources also drives the lower seasonal variability here compared to the tropical Atlantic, where BB influence peaks in June–August and October–November, characterized by high  $\text{O}_3$  ( $> 75$  ppbv) and high CO ( $> 100$  ppbv) (Fig. 13f), significantly increases the  $\text{O}_3$  vertical distribution compared to the other seasons (Figs. 12c, 12h, and 12m). Finally, photochemistry, which regulates  $\text{O}_3$  net balance in the troposphere, is less seasonally variable in the tropics than in the extra-tropics, where the photolysis frequency of  $\text{O}_3$  ( $j(\text{O}_3)$ ) and photochemical production of  $\text{O}_3$  fluctuate annually with solar zenith angle.

**$\text{O}_3$  minima and maxima.** Coincident  $\text{O}_3$  and CO enhancements were observed in the tropical Atlantic for each ATom circuit (Figs. 9 and 13f), suggesting a year-round influence of continental emissions and distinctive dynamics in this region (Krishnamurti et al., 1996; Thompson et al., 1996). In the tropical Pacific, the April–May period stands out due to an  $\text{O}_3$  and CO enhancement episode during HIPPO (Fig. 9) that was attributed to the transport of anthropogenic and BB emissions from southeast Asia (Shen et al., 2014). Deep convection in the tropics brings  $\text{O}_3$ -poor ( $< 15$  ppbv) air to the upper troposphere (Kley et al., 1996; Pan et al., 2015; Solomon et al., 2005). However, the spatial extent of these events remains poorly constrained. Results from ATom and HIPPO suggest that deep convection can loft  $\text{O}_3$ -poor air at least up to 12 km (the altitude ceiling of this study) in the tropical Pacific, and occurred more frequently between January and May (Figs. 12c and h). During the rest of the year,  $\text{O}_3$ -poor air was typically confined below 4 km. Conversely,  $\text{O}_3$ -poor air is confined to the first 2 km in the tropical Atlantic (Fig. S5). Meteorological analysis of tropical ozonesondes shows that subsidence of higher- $\text{O}_3$  air aloft over the Atlantic is one reason  $\text{O}_3$ -poor air is found only in the boundary layer (Thompson et al., 2000, 2012).

#### 4.2. Middle- and high-latitudes

**Vertical distribution.** In the middle- and high-latitudes, tropospheric  $\text{O}_3$  was generally at a minimum in the MBL and increased with altitude. Above 8 km, increasing  $\text{O}_3$  with altitude



(Figs. 10b–e) and its persistent anticorrelation with CO (Fig. 13) points to stratospheric air sampling as the cause for higher O<sub>3</sub> variability in the extra-tropical UTLS, especially at high latitudes where the tropopause is lower and wave breaking of the polar jet streams can lead to stratospheric intrusions. As a result, the  $S_{score}$  decrease above 8 km, summarized in Figure 11a, is ascribed to variability in the influence of stratospheric air. ATom detected little change in the O<sub>3</sub> distribution over the Pacific Ocean since HIPPO, with a  $S_{score}$  averaging 74 % in the 0–8 km range. The relative difference between median O<sub>3</sub> values from HIPPO and ATom in the Pacific is generally lower than 20 % (Fig. 11b). Similarly, the relative difference between median O<sub>3</sub> mixing ratios between ATom Atlantic and Pacific below 8 km is consistently lower than 20 %, with an average  $S_{score}$  of 75 % between (Fig. 11b). The southern high-latitudes are the only region where the  $S_{score}$  below 8 km occasionally fell below 60 % (Fig. 10e). However, a lower  $S_{score}$  was expected there as the Atlantic vertical profile is based on only two seasonal flights to Antarctica, whereas there were four seasonal flights in the Pacific. Additionally, HIPPO was less spatially extensive – resulting in fewer data points – in this latitude bin compared to ATom (Fig. 1), which could explain the low  $S_{score}$  values when comparing the two missions (Fig. 10e). Nevertheless, the similar O<sub>3</sub> distribution in the extra-tropical free troposphere above the two oceans is consistent with an O<sub>3</sub> lifetime sufficiently long for rapid zonal transport to smooth out variations in baseline O<sub>3</sub> distribution in the remote troposphere, across a relatively wide range of longitudes (Figs. 10b–e). The comparison of O<sub>3</sub> seasonal cycles at remote ozonesonde launching sites of the northern midlatitudes yields similar results and further supports this conclusion (Logan, 1985; Parrish et al., 2020). Studies of the spatial representativeness of tropospheric O<sub>3</sub> monitoring networks have concluded that tropospheric O<sub>3</sub> distributions varied significantly with longitude, especially in the northern middle- and high-latitudes over continents (Liu et al., 2013; Tilmes et al., 2012). ATom findings stem from O<sub>3</sub> measurements predominantly over the oceans, possibly yielding a different picture of O<sub>3</sub> longitudinal distribution away from regional precursor emissions.

**Seasonality.** The extra-tropical vertical profiles of O<sub>3</sub> vary seasonally during ATom and HIPPO. The summer season in the middle- and high-latitudes was remarkable over both oceans and hemispheres for the steep O<sub>3</sub> gradients in the tropospheric column (Fig. 12 in black). In the MBL, median O<sub>3</sub> was consistently under 25 ppbv in the summer, whereas O<sub>3</sub> was over 25 ppbv in other seasons. Low O<sub>3</sub> in the MBL in summer reflects the enhanced O<sub>3</sub> photochemical

destruction in this NO<sub>x</sub>-limited region. Photochemical destruction decreases in dry air in the upper troposphere, thus leading to the steep O<sub>3</sub> gradients observed here. The summer O<sub>3</sub> minimum was especially apparent in the high latitudes of the southern Pacific during ATom and extended well above the MBL into the free troposphere (Fig. 12 in black).

O<sub>3</sub> mixing ratios were highest in the tropospheric column during springtime in both hemispheres, and over both oceans (Fig. 12 in gold). A notable exception occurred during springtime in the high latitudes of the NH, where several O<sub>3</sub> depletion events were sampled in the lower legs of the Arctic transit. During these events, O<sub>3</sub> mixing ratios lower than 10 ppbv were measured, resulting in a lower 25<sup>th</sup> percentile of O<sub>3</sub> distribution at the lowest altitude compared to the other seasons (Fig. 12e in gold). A tropospheric O<sub>3</sub> springtime maximum has often been reported in the NH (e.g., Monks, 2000) when meteorology favors efficient transport of O<sub>3</sub> and precursors from continental air from North America and Eurasia (Owen et al., 2006; Zhang et al., 2017, 2008). Another contributing factor is the increased frequency of stratospheric air mixing in spring that significantly contributes to higher O<sub>3</sub> levels (Lin et al., 2015b; Tarasick et al., 2019b). Further, the tropospheric O<sub>3</sub> springtime maximum in the SH is often attributed to BB emissions reaching a peak ((Fishman et al., 1991; Gaudel et al., 2018), but stratospheric air mixing also occurs (Diab et al., 1996, 2004; Greenslade et al., 2017). Here, the O<sub>3</sub>/CO relationship in spring shows that the enhanced stratospheric mixing with tropospheric air during this season, both in the northern and southern middle- and high-latitudes, contributes to the increase in column O<sub>3</sub> (Fig. 13).

Fall and winter seasons shared similar features in the middle- and high-latitudes: no strong O<sub>3</sub> gradient was measured in the free troposphere, and O<sub>3</sub> values varied over similar ranges – about 40 ppbv in the NH and about 30 ppbv in the SH – during the two seasons (Fig. 12 in red and blue).

**O<sub>3</sub> enhancements.** The linear increase of O<sub>3</sub> with CO >100 ppbv highlights the contribution of natural and anthropogenic pollution plumes lofted from continental areas into the remote troposphere.

In the NH, these events occur almost year-round (Figs. 13b–c and 13g–h). Higher CO enhancements in the Pacific (Figs. 13g–h) than in the Atlantic (Figs. 13b–c) have been observed before and attributed to sampling bias (Clark et al., 2015). Here, our findings suggest a year-round influence of continental emissions on the Pacific atmosphere despite its remoteness.

Modeled back trajectories show that most air masses sampled in the NH during ATom were influenced by long-range transport of continental emissions from Asia, Africa, and North America (Fig. S6). Previous studies have shown anthropogenic and BB emission outflow from Asia significantly contributed to O<sub>3</sub> pollution events measured over the northern Pacific or in California (e.g., Heald et al., 2003; Jaffe et al., 2004; Lin et al., 2017). Intercontinental transport of anthropogenic emissions from Europe can also contribute to the Asian outflow of anthropogenic pollution (e.g., Bey et al., 2001; Liu et al., 2002; Newell and Evans, 2000). Finally, O<sub>3</sub> enhancements in the northern Atlantic were frequently observed and attributed to midlatitude anthropogenic and boreal forest fire emissions (e.g., Honrath et al., 2004; Martín et al., 2006; Trickl et al., 2003).

In the SH, polluted air is encountered more often in spring and summer over the Atlantic, but springtime CO is greater than in other seasons over the Pacific (Figs. 13d–e and 13i–j). During spring, median O<sub>3</sub> above 50 ppbv was measured throughout the free troposphere in the southern midlatitudes (Fig. 12). Several air masses intercepted during these flights originated from regions that were intensively burning at the time, notably equatorial and southern Africa, Australia, and southern South America, contributing to the observed enhanced O<sub>3</sub> and CO (Fig. S4).

## 5. Conclusion

We present tropospheric O<sub>3</sub> distributions measured over remote regions of the Pacific and Atlantic Oceans during two airborne chemical sampling projects: the four deployments of ATom (2016–2018) and the five deployments of HIPPO (2009–2011). The data highlight several regional- and large-scale features of O<sub>3</sub> distributions, and provide ~~valuable new~~ insight into ~~current~~ O<sub>3</sub> distributions in remote regions. The main findings are as follows:

- ATom and HIPPO provide a unique perspective on vertically-resolved global baseline O<sub>3</sub> distributions over the Pacific and Atlantic basins, and expand upon spatially-limited O<sub>3</sub> climatologies from long-term datasets to highlight large-scale features necessary for model output and satellite retrieval validation.
- ATom and HIPPO O<sub>3</sub> data are consistent – where they overlap – with measurement-based climatologies of tropospheric O<sub>3</sub> from well-established ozonesonde and commercial aircraft monitoring programs. ATom and HIPPO seasonal median O<sub>3</sub> showed

high correlation ( $R^2 > 0.7$ ) with corresponding seasonal median  $O_3$  from ozonesondes, giving confidence in the accurate depiction of the emerging global  $O_3$  climatology by these diverse research activities. ATom and HIPPO captured 30–71 % of  $O_3$  variability measured by ozonesondes launched in the vicinity of the aircraft flight tracks, and had the same mode of the  $O_3$  distribution as determined by IAGOS in the northern Atlantic UTLS.

- Higher  $O_3$  loading in the NH compared to the SH is consistent with the heterogeneous distribution of  $O_3$  precursor emissions around the globe, mostly concentrated in the NH, a result consistent with previous modeling studies and satellite observations. ATom Atlantic vs. Pacific comparison reveals a similar  $O_3$  distribution in the free troposphere up to ~8 km in the middle- and high-latitudes, but not in the tropics. Similar  $O_3$  distributions across latitude bands have been suggested in the past, but these studies were limited to the northern midlatitudes. Conversely, other observation-based studies indicated significant  $O_3$  longitudinal gradients. Here, our findings are consistent with zonal transport smoothing the baseline  $O_3$  distribution longitudinally from the Pacific to the Atlantic. In the tropics, median  $O_3$  mixing ratios are about twice as high in the Atlantic than in the Pacific, due to a well-documented mixture of dynamical patterns interacting with the transport of continental air masses.
- A comparison of seasonal  $O_3$  vertical profiles did not reveal a marked seasonality in the tropics, but instead highlighted the influence of specific events, most notably BB emissions from Africa and South America, which have been extensively documented in the literature. In the extra-tropics, the summer season was characterized by a steeper tropospheric  $O_3$  gradient driven by very low  $O_3$  abundance in the MBL. Fall and winter seasons generally led to near-constant  $O_3$  mixing ratios from the surface to the upper troposphere, while the highest  $O_3$  abundance was recorded during the spring season when more frequent and intense stratospheric intrusions and transport of air masses from continental regions occur. ATom and HIPPO provide the first airborne in situ vertically-resolved  $O_3$  climatology covering both the Atlantic and Pacific Oceans in the NH and in the SH. They confirm and extend the current understanding of  $O_3$  variability in the remote troposphere, built over several decades by airborne campaigns, monitoring networks, and satellite observations.

- Overall, this paper highlights the value of the ATom and HIPPO datasets, which cover spatial scales commensurate with the grid resolution of current Earth system models, and further useful as a priori estimates for improved retrievals of tropospheric O<sub>3</sub> from satellite remote sensing platforms. **In addition, ATom and HIPPO in situ measurements help to establish the quantitative legacy of global pollution transport and chemistry by through the evaluation of key, covarying species – in this case O<sub>3</sub> and CO.** ATom and HIPPO datasets should be critical for improving the scientific community's understanding of O<sub>3</sub> production and loss processes, and the influence of anthropogenic emissions on baseline O<sub>3</sub> in remote regions. They provide a timely addition to the Tropospheric Ozone Assessment Report (TOAR) effort to characterize the global-scale O<sub>3</sub> distribution, and address some of the measurement gaps identified therein.

## Acknowledgments

We thank the ATom leadership team, science team, and DC-8 pilots and crew for contributions to the ATom measurements. ATom was funded in response to NASA ROSES-2013 NRA NNN13ZDA001N-EVS2. The authors acknowledge support by the U.S. National Oceanic and Atmospheric Administration (NOAA) Health of the Atmosphere and Atmospheric Chemistry, Carbon Cycle, and Climate Programs. SHADOZ ozonesondes are supported by the Upper Atmosphere Research Program of NASA. Ozonesoundings at Marambio have been supported by the Finnish Antarctic research program (FINNARP). The IAGOS program acknowledges the European Commission for its support of the MOZAIC project (1994-2003) the preparatory phase of IAGOS (2005-2013) and IGAS (2013-2016); the partner institutions of the IAGOS Research Infrastructure (FZJ, DLR, MPI, KIT in Germany, CNRS, Météo-France, Université Paul Sabatier in France, and University of Manchester, UK); the French Atmospheric Data Center AERIS for hosting the database; and the participating airlines (Lufthansa, Air France, China Airlines, Iberia, Cathay Pacific, Hawaiian Airlines) for transporting the instrumentation free of charge. We thank J. A. Neuman, H. Angot, and O. Cooper for helpful discussions and careful editing of this manuscript.

## References

622 Andreae, M. O., Anderson, B. E., Blake, D. R., Bradshaw, J. D., Collins, J. E., Gregory, G. L.,  
 623 Sachse, G. W. and Shipham, M. C.: Influence of plumes from biomass burning on atmospheric  
 624 chemistry over the equatorial and tropical South Atlantic during CITE 3, *Journal of Geophysical*  
 625 *Research*, 99(D6), 12793, doi:10.1029/94JD00263, 1994.

626 Bey, I., Jacob, D. J., Logan, J. A. and Yantosca, R. M.: Asian chemical outflow to the Pacific in  
 627 spring: Origins, pathways, and budgets, *Journal of Geophysical Research: Atmospheres*,  
 628 106(D19), 23097–23113, doi:10.1029/2001JD000806, 2001.

629 Bowman, K. P.: Large-scale isentropic mixing properties of the Antarctic polar vortex from  
 630 analyzed winds, *Journal of Geophysical Research: Atmospheres*, 98(D12), 23013–23027,  
 631 doi:10.1029/93JD02599, 1993.

632 Bowman, K. P. and Carrie, G. D.: The Mean-Meridional Transport Circulation of the Troposphere  
 633 in an Idealized GCM, *J. Atmos. Sci.*, 59(9), 1502–1514, doi:10.1175/1520-  
 634 0469(2002)059<1502:TMMTCO>2.0.CO;2, 2002.

635 Brenninkmeijer, C. a. M., Crutzen, P., Boumard, F., Dauer, T., Dix, B., Ebinghaus, R., Filippi, D.,  
 636 Fischer, H., Franke, H., Frieß, U., Heintzenberg, J., Helleis, F., Hermann, M., Kock, H. H., Koepfel,  
 637 C., Lelieveld, J., Leuenberger, M., Martinsson, B. G., Miemczyk, S., Moret, H. P., Nguyen, H. N.,  
 638 Nyfeler, P., Oram, D., O’Sullivan, D., Penkett, S., Platt, U., Pupek, M., Ramonet, M., Randa, B.,  
 639 Reichelt, M., Rhee, T. S., Rohwer, J., Rosenfeld, K., Scharffe, D., Schlager, H., Schumann, U.,  
 640 Slemr, F., Sprung, D., Stock, P., Thaler, R., Valentino, F., Velthoven, P. van, Waibel, A., Wandel,  
 641 A., Waschitschek, K., Wiedensohler, A., Xueref-Remy, I., Zahn, A., Zech, U. and Ziereis, H.: Civil  
 642 Aircraft for the regular investigation of the atmosphere based on an instrumented container:  
 643 The new CARIBIC system, *Atmospheric Chemistry and Physics*, 7(18), 4953–4976,  
 644 doi:https://doi.org/10.5194/acp-7-4953-2007, 2007.

645 Browell, E. V., Fenn, M. A., Butler, C. F., Grant, W. B., Merrill, J. T., Newell, R. E., Bradshaw, J. D.,  
 646 Sandholm, S. T., Anderson, B. E., Bandy, A. R., Bachmeier, A. S., Blake, D. R., Davis, D. D.,  
 647 Gregory, G. L., Heikes, B. G., Kondo, Y., Liu, S. C., Rowland, F. S., Sachse, G. W., Singh, H. B.,  
 648 Talbot, R. W. and Thornton, D. C.: Large-scale air mass characteristics observed over western  
 649 Pacific during summertime, *Journal of Geophysical Research: Atmospheres*, 101(D1), 1691–  
 650 1712, doi:10.1029/95JD02200, 1996a.

651 Browell, E. V., Fenn, M. A., Butler, C. F., Grant, W. B., Clayton, M. B., Fishman, J., Bachmeier, A.  
 652 S., Anderson, B. E., Gregory, G. L., Fuelberg, H. E., Bradshaw, J. D., Sandholm, S. T., Blake, D. R.,  
 653 Heikes, B. G., Sachse, G. W., Singh, H. B. and Talbot, R. W.: Ozone and aerosol distributions and  
 654 air mass characteristics over the South Atlantic Basin during the burning season, *Journal of*  
 655 *Geophysical Research: Atmospheres*, 101(D19), 24043–24068, doi:10.1029/95JD02536, 1996b.

656 Clark, H., Sauvage, B., Thouret, V., Nédélec, P., Blot, R., Wang, K.-Y., Smit, H., Neis, P., Petzold,  
 657 A., Athier, G., Boulanger, D., Cousin, J.-M., Beswick, K., Gallagher, M., Baumgardner, D., Kaiser,  
 658 J., Flaud, J.-M., Wahner, A., Volz-Thomas, A. and Cammas, J.-P.: The first regular measurements

659 of ozone, carbon monoxide and water vapour in the Pacific UTLS by IAGOS, *Tellus B: Chemical*  
660 *and Physical Meteorology*, 67(1), 28385, doi:10.3402/tellusb.v67.28385, 2015.

661 Cohen, Y., Petetin, H., Thouret, V., Marécal, V., Josse, B., Clark, H., Sauvage, B., Fontaine, A.,  
662 Athier, G., Blot, R., Boulanger, D., Cousin, J.-M. and Nédélec, P.: Climatology and long-term  
663 evolution of ozone and carbon monoxide in the upper troposphere–lower stratosphere (UTLS)  
664 at northern midlatitudes, as seen by IAGOS from 1995 to 2013, *Atmospheric Chemistry and*  
665 *Physics*, 18(8), 5415–5453, doi:https://doi.org/10.5194/acp-18-5415-2018, 2018.

666 Cooper, O. R., Stohl, A., Hübler, G., Hsie, E. Y., Parrish, D. D., Tuck, A. F., Kiladis, G. N., Oltmans,  
667 S. J., Johnson, B. J., Shapiro, M., Moody, J. L. and Lefohn, A. S.: Direct transport of midlatitude  
668 stratospheric ozone into the lower troposphere and marine boundary layer of the tropical  
669 Pacific Ocean, *J. Geophys. Res.*, 110(D23), D23310, doi:10.1029/2005JD005783, 2005.

670 Cooper, O. R., Parrish, D. D., Ziemke, J., Balashov, N. V., Cupeiro, M., Galbally, I. E., Gilge, S.,  
671 Horowitz, L., Jensen, N. R., Lamarque, J.-F., Naik, V., Oltmans, S. J., Schwab, J., Shindell, D. T.,  
672 Thompson, A. M., Thouret, V., Wang, Y. and Zbinden, R. M.: Global distribution and trends of  
673 tropospheric ozone: An observation-based review, *Elem Sci Anth*, 2(0),  
674 doi:10.12952/journal.elementa.000029, 2014.

675 Crawford, J., Davis, D., Chen, G., Bradshaw, J., Sandholm, S., Kondo, Y., Liu, S., Browell, E.,  
676 Gregory, G., Anderson, B., Sachse, G., Collins, J., Barrick, J., Blake, D., Talbot, R. and Singh, H.: An  
677 assessment of ozone photochemistry in the extratropical western North Pacific: Impact of  
678 continental outflow during the late winter/early spring, *Journal of Geophysical Research:*  
679 *Atmospheres*, 102(D23), 28469–28487, doi:10.1029/97JD02600@10.1002/(ISSN)2169-  
680 8996.PEMWEST1, 1997.

681 Crutzen, P. J.: Photochemical reactions initiated by and influencing ozone in unpolluted  
682 tropospheric air, *Tellus*, 26(1–2), 47–57, doi:10.3402/tellusa.v26i1-2.9736, 1974.

683 Davis, D. D., Crawford, J., Chen, G., Chameides, W., Liu, S., Bradshaw, J., Sandholm, S., Sachse,  
684 G., Gregory, G., Anderson, B., Barrick, J., Bachmeier, A., Collins, J., Browell, E., Blake, D.,  
685 Rowland, S., Kondo, Y., Singh, H., Talbot, R., Heikes, B., Merrill, J., Rodriguez, J. and Newell, R.  
686 E.: Assessment of ozone photochemistry in the western North Pacific as inferred from PEM-  
687 West A observations during the fall 1991, *Journal of Geophysical Research: Atmospheres*,  
688 101(D1), 2111–2134, doi:10.1029/95JD02755, 1996.

689 Derwent, R. G., Parrish, D. D., Galbally, I. E., Stevenson, D. S., Doherty, R. M., Young, P. J. and  
690 Shallcross, D. E.: Interhemispheric differences in seasonal cycles of tropospheric ozone in the  
691 marine boundary layer: Observation-model comparisons, *Journal of Geophysical Research:*  
692 *Atmospheres*, 121(18), 11,075–11,085, doi:10.1002/2016JD024836, 2016.

693 Diab, R. D., Thompson, A. M., Zunckel, M., Coetzee, G. J. R., Combrink, J., Bodeker, G. E.,  
694 Fishman, J., Sokolic, F., McNamara, D. P., Archer, C. B. and Nganga, D.: Vertical ozone

695 distribution over southern Africa and adjacent oceans during SAFARI-92, *Journal of Geophysical*  
696 *Research: Atmospheres*, 101(D19), 23823–23833, doi:10.1029/96JD01267, 1996.

697 Diab, R. D., Thompson, A. M., Mari, K., Ramsay, L. and Coetzee, G. J. R.: Tropospheric ozone  
698 climatology over Irene, South Africa, from 1990 to 1994 and 1998 to 2002, *Journal of*  
699 *Geophysical Research: Atmospheres*, 109(D20), doi:10.1029/2004JD004793, 2004.

700 Edwards, D. P., Lamarque, J.-F., Attié, J.-L., Emmons, L. K., Richter, A., Cammas, J.-P., Gille, J. C.,  
701 Francis, G. L., Deeter, M. N., Warner, J., Ziskin, D. C., Lyjak, L. V., Drummond, J. R. and Burrows,  
702 J. P.: Tropospheric ozone over the tropical Atlantic: A satellite perspective, *Journal of*  
703 *Geophysical Research: Atmospheres*, 108(D8), doi:10.1029/2002JD002927, 2003.

704 Fan, S.-M. and Jacob, D. J.: Surface ozone depletion in Arctic spring sustained by bromine  
705 reactions on aerosols, *Nature*, 359(6395), 522–524, doi:10.1038/359522a0, 1992.

706 Fenn, M. A., Browell, E. V., Butler, C. F., Grant, W. B., Kooi, S. A., Clayton, M. B., Gregory, G. L.,  
707 Newell, R. E., Zhu, Y., Dibb, J. E., Fuelberg, H. E., Anderson, B. E., Bandy, A. R., Blake, D. R.,  
708 Bradshaw, J. D., Heikes, B. G., Sachse, G. W., Sandholm, S. T., Singh, H. B., Talbot, R. W. and  
709 Thornton, D. C.: Ozone and aerosol distributions and air mass characteristics over the South  
710 Pacific during the burning season, *Journal of Geophysical Research: Atmospheres*, 104(D13),  
711 16197–16212, doi:10.1029/1999JD900065, 1999.

712 Fishman, J., Watson, C. E., Larsen, J. C. and Logan, J. A.: Distribution of tropospheric ozone  
713 determined from satellite data, *Journal of Geophysical Research: Atmospheres*, 95(D4), 3599–  
714 3617, doi:10.1029/JD095iD04p03599, 1990.

715 Fishman, J., Fakhruzzaman, K., Cros, B. and Nganga, D.: Identification of Widespread Pollution in  
716 the Southern Hemisphere Deduced from Satellite Analyses, *Science*, 252(5013), 1693–1696,  
717 doi:10.1126/science.252.5013.1693, 1991.

718 Fishman, J., Hoell, J. M., Bendura, R. D., McNeal, R. J. and Kirchhoff, V. W. J. H.: NASA GTE  
719 TRACE A experiment (September–October 1992): Overview, *Journal of Geophysical Research:*  
720 *Atmospheres*, 101(D19), 23865–23879, doi:10.1029/96JD00123, 1996.

721 Gaudel, A., Clark, H., Thouret, V., Jones, L., Inness, A., Flemming, J., Stein, O., Huijnen, V., Eskes,  
722 H., Nedelec, P. and Boulanger, D.: On the use of MOZAIC-IAgos data to assess the ability of the  
723 MACC reanalysis to reproduce the distribution of ozone and CO in the UTLS over Europe, *Tellus*  
724 *B: Chemical and Physical Meteorology*, 68(s1), 27955, doi:10.3402/tellusb.v67.27955, 2015.

725 Gaudel, A., Cooper, O. R., Ancellet, G., Barret, B., Boynard, A., Burrows, J. P., Clerbaux, C.,  
726 Coheur, P.-F., Cuesta, J., Cuevas, E., Doniki, S., Dufour, G., Ebojie, F., Foret, G., Garcia, O.,  
727 Muños, M. J. G., Hannigan, J. W., Hase, F., Huang, G., Hassler, B., Hurtmans, D., Jaffe, D., Jones,  
728 N., Kalabokas, P., Kerridge, B., Kulawik, S. S., Latter, B., Leblanc, T., Flochmoën, E. L., Lin, W., Liu,  
729 J., Liu, X., Mahieu, E., McClure-Begley, A., Neu, J. L., Osman, M., Palm, M., Petetin, H.,  
730 Petropavlovskikh, I., Querel, R., Raphe, N., Rozanov, A., Schultz, M. G., Schwab, J., Siddans, R.,



731 Smale, D., Steinbacher, M., Tanimoto, H., Tarasick, D. W., Thouret, V., Thompson, A. M., Trickl,  
 732 T., Weatherhead, E., Wespes, C., Worden, H. M., Vigouroux, C., Xu, X., Zeng, G. and Ziemke, J.:  
 733 Tropospheric Ozone Assessment Report: Present-day distribution and trends of tropospheric  
 734 ozone relevant to climate and global atmospheric chemistry model evaluation, *Elem Sci Anth*,  
 735 6(1), doi:10.1525/elementa.291, 2018.

736 Greenslade, J. W., Alexander, S. P., Schofield, R., Fisher, J. A. and Klekociuk, A. K.: Stratospheric  
 737 ozone intrusion events and their impacts on tropospheric ozone in the Southern Hemisphere,  
 738 *Atmospheric Chemistry and Physics*, 17(17), 10269–10290, doi:10.5194/acp-17-10269-2017,  
 739 2017.

740 Heald, C. L., Jacob, D. J., Fiore, A. M., Emmons, L. K., Gille, J. C., Deeter, M. N., Warner, J.,  
 741 Edwards, D. P., Crawford, J. H., Hamlin, A. J., Sachse, G. W., Browell, E. V., Avery, M. A., Vay, S.  
 742 A., Westberg, D. J., Blake, D. R., Singh, H. B., Sandholm, S. T., Talbot, R. W. and Fuelberg, H. E.:  
 743 Asian outflow and trans-Pacific transport of carbon monoxide and ozone pollution: An  
 744 integrated satellite, aircraft, and model perspective, *Journal of Geophysical Research:*  
 745 *Atmospheres*, 108(D24), doi:10.1029/2003JD003507, 2003.

746 Holmes, C. D., Prather, M. J., Søvde, O. A. and Myhre, G.: Future methane, hydroxyl, and their  
 747 uncertainties: key climate and emission parameters for future predictions, *Atmos. Chem. Phys.*,  
 748 13(1), 285–302, doi:10.5194/acp-13-285-2013, 2013.

749 Honrath, R. E., Owen, R. C., Martín, M. V., Reid, J. S., Lapina, K., Fialho, P., Dziobak, M. P., Kleissl,  
 750 J. and Westphal, D. L.: Regional and hemispheric impacts of anthropogenic and biomass burning  
 751 emissions on summertime CO and O<sub>3</sub> in the North Atlantic lower free troposphere, *Journal of*  
 752 *Geophysical Research: Atmospheres*, 109(D24), doi:10.1029/2004JD005147, 2004.

753 Hu, L., Jacob, D. J., Liu, X., Zhang, Y., Zhang, L., Kim, P. S., Sulprizio, M. P. and Yantosca, R. M.:  
 754 Global budget of tropospheric ozone: Evaluating recent model advances with satellite (OMI),  
 755 aircraft (IAGOS), and ozonesonde observations, *Atmospheric Environment*, 167, 323–334,  
 756 doi:10.1016/j.atmosenv.2017.08.036, 2017.

757 IPCC: Climate Change 2013: The Physical Science Basis. Contribution of Working Group I to the  
 758 Fifth Assessment Report of the Intergovernmental Panel on Climate Change, Cambridge  
 759 University Press, Cambridge, United Kingdom and New York, NY, USA. [online] Available from:  
 760 <https://www.ipcc.ch/report/ar5/wg1/> (Accessed 8 January 2019), 2013.

761 Jacob, D. J., Heikes, E. G., Fan, S.-M., Logan, J. A., Mauzerall, D. L., Bradshaw, J. D., Singh, H. B.,  
 762 Gregory, G. L., Talbot, R. W., Blake, D. R. and Sachse, G. W.: Origin of ozone and NO<sub>x</sub> in the  
 763 tropical troposphere: A photochemical analysis of aircraft observations over the South Atlantic  
 764 basin, *Journal of Geophysical Research: Atmospheres*, 101(D19), 24235–24250,  
 765 doi:10.1029/96JD00336, 1996.

766 Jaffe, D., Bertschi, I., Jaeglé, L., Novelli, P., Reid, J. S., Tanimoto, H., Vingarzan, R. and Westphal,  
 767 D. L.: Long-range transport of Siberian biomass burning emissions and impact on surface ozone

768 in western North America, *Geophysical Research Letters*, 31(16), doi:10.1029/2004GL020093,  
769 2004.

770 Jensen, A. A., Thompson, A. M. and Schmidlin, F. J.: Classification of Ascension Island and Natal  
771 ozonesondes using self-organizing maps, *Journal of Geophysical Research: Atmospheres*,  
772 117(D4), doi:10.1029/2011JD016573, 2012.

773 Jourdain, L., Worden, H. M., Worden, J. R., Bowman, K., Li, Q., Eldering, A., Kulawik, S. S.,  
774 Osterman, G., Boersma, K. F., Fisher, B., Rinsland, C. P., Beer, R. and Gunson, M.: Tropospheric  
775 vertical distribution of tropical Atlantic ozone observed by TES during the northern African  
776 biomass burning season, *Geophysical Research Letters*, 34(4), doi:10.1029/2006GL028284,  
777 2007.

778 Junge, C. E.: Global ozone budget and exchange between stratosphere and troposphere, *Tellus*,  
779 14(4), 363–377, doi:10.1111/j.2153-3490.1962.tb01349.x, 1962.

780 Karion, A., Sweeney, C., Wolter, S., Newberger, T., Chen, H., Andrews, A., Kofler, J., Neff, D. and  
781 Tans, P.: Long-term greenhouse gas measurements from aircraft, *Atmospheric Measurement*  
782 *Techniques*, 6(3), 511–526, doi:https://doi.org/10.5194/amt-6-511-2013, 2013.

783 Katich, J. M., Samset, B. H., Bui, T. P., Dollner, M., Froyd, K. D., Campuzano-Jost, P., Nault, B. A.,  
784 Schroder, J. C., Weinzierl, B. and Schwarz, J. P.: Strong Contrast in Remote Black Carbon Aerosol  
785 Loadings Between the Atlantic and Pacific Basins, *Journal of Geophysical Research:*  
786 *Atmospheres*, 123(23), 13,386–13,395, doi:10.1029/2018JD029206, 2018.

787 Kley, D., Crutzen, P. J., Smit, H. G. J., Vömel, H., Oltmans, S. J., Grassl, H. and Ramanathan, V.:  
788 Observations of Near-Zero Ozone Concentrations Over the Convective Pacific: Effects on Air  
789 Chemistry, *Science*, 274(5285), 230–233, doi:10.1126/science.274.5285.230, 1996.

790 Komhyr, W.: Electrochemical Concentration Cells for Gas Analysis, *Annales De Geophysique*,  
791 25(1), 203–, 1969.

792 Kondo, Y., Morino, Y., Takegawa, N., Koike, M., Kita, K., Miyazaki, Y., Sachse, G. W., Vay, S. A.,  
793 Avery, M. A., Flocke, F., Weinheimer, A. J., Eisele, F. L., Zondlo, M. A., Weber, R. J., Singh, H. B.,  
794 Chen, G., Crawford, J., Blake, D. R., Fuelberg, H. E., Clarke, A. D., Talbot, R. W., Sandholm, S. T.,  
795 Browell, E. V., Streets, D. G. and Liley, B.: Impacts of biomass burning in Southeast Asia on  
796 ozone and reactive nitrogen over the western Pacific in spring, *Journal of Geophysical Research:*  
797 *Atmospheres*, 109(D15), doi:10.1029/2003JD004203, 2004.

798 Krishnamurti, T. N., Sinha, M. C., Kanamitsu, M., Oosterhof, D., Fuelberg, H., Chatfield, R., Jacob,  
799 D. J. and Logan, J.: Passive tracer transport relevant to the TRACE A experiment, *Journal of*  
800 *Geophysical Research: Atmospheres*, 101(D19), 23889–23907, doi:10.1029/95JD02419, 1996.

801 Leonard, M., Petropavlovskikh, I., Lin, M., McClure-Begley, A., Johnson, B. J., Oltmans, S. J. and  
802 Tarasick, D.: An assessment of 10-year NOAA aircraft-based tropospheric ozone profiling in

803 Colorado, Atmospheric Environment, 158, 116–127, doi:10.1016/j.atmosenv.2017.03.013,  
804 2017.

805 Levy, H.: Normal Atmosphere: Large Radical and Formaldehyde Concentrations Predicted,  
806 Science, 173(3992), 141–143, doi:10.1126/science.173.3992.141, 1971.

807 Lin, M., Fiore, A. M., Horowitz, L. W., Langford, A. O., Oltmans, S. J., Tarasick, D. and Rieder, H.  
808 E.: Climate variability modulates western US ozone air quality in spring via deep stratospheric  
809 intrusions, Nature Communications, 6, 7105, doi:10.1038/ncomms8105, 2015b.

810 Lin, M., Horowitz, L. W., Cooper, O. R., Tarasick, D. W., Conley, S., Iraci, L. T., Johnson, B. J.,  
811 Leblanc, T., Petropavlovskikh, I. and Yates, E. L.: Revisiting the evidence of increasing springtime  
812 ozone mixing ratios in the free troposphere over western North America, Geophysical Research  
813 Letters, 42(20), 8719–8728, doi:10.1002/2015GL065311, 2015a.

814 Lin, M., Horowitz, L. W., Payton, R., Fiore, A. M. and Tonnesen, G.: US surface ozone trends and  
815 extremes from 1980 to 2014: quantifying the roles of rising Asian emissions, domestic controls,  
816 wildfires, and climate, Atmospheric Chemistry and Physics, 17(4), 2943–2970, doi:10.5194/acp-  
817 17-2943-2017, 2017.

818 Liu, G., Tarasick, D. W., Fioletov, V. E., Sioris, C. E. and Rochon, Y. J.: Ozone correlation lengths  
819 and measurement uncertainties from analysis of historical ozonesonde data in North America  
820 and Europe, Journal of Geophysical Research: Atmospheres, 114(D4),  
821 doi:10.1029/2008JD010576, 2009.

822 Liu, G., Liu, J., Tarasick, D. W., Fioletov, V. E., Jin, J. J., Moeini, O., Liu, X., Sioris, C. E. and Osman,  
823 M.: A global tropospheric ozone climatology from trajectory-mapped ozone soundings,  
824 Atmospheric Chemistry and Physics, 13(21), 10659–10675, doi:10.5194/acp-13-10659-2013,  
825 2013.

826 Liu, H., Jacob, D. J., Chan, L. Y., Oltmans, S. J., Bey, I., Yantosca, R. M., Harris, J. M., Duncan, B. N.  
827 and Martin, R. V.: Sources of tropospheric ozone along the Asian Pacific Rim: An analysis of  
828 ozonesonde observations, Journal of Geophysical Research: Atmospheres, 107(D21), ACH 3-1-  
829 ACH 3-19, doi:10.1029/2001JD002005, 2002.

830 Logan, J. A.: Tropospheric ozone: Seasonal behavior, trends, and anthropogenic influence,  
831 Journal of Geophysical Research: Atmospheres, 90(D6), 10463–10482,  
832 doi:10.1029/JD090iD06p10463, 1985.

833 Logan, J. A. and Kirchhoff, V. W. J. H.: Seasonal variations of tropospheric ozone at Natal, Brazil,  
834 Journal of Geophysical Research: Atmospheres, 91(D7), 7875–7881,  
835 doi:10.1029/JD091iD07p07875, 1986.

836 Logan, J. A., Staehelin, J., Megretskaia, I. A., Cammas, J. -P., Thouret, Claude, H., Backer, H.,  
837 Steinbacher, M., Scheel, H. -E., Stübi, R., Fröhlich, M. and Derwent, R.: Changes in ozone over  
838 Europe: Analysis of ozone measurements from sondes, regular aircraft (MOZAIC) and alpine

839 surface sites, *Journal of Geophysical Research: Atmospheres*, 117(D9),  
840 doi:10.1029/2011JD016952, 2012.

841 Marenco, A., Thouret, V., Nédélec, P., Smit, H., Helten, M., Kley, D., Karcher, F., Simon, P., Law,  
842 K., Pyle, J., Poschmann, G., Wrede, R. V., Hume, C. and Cook, T.: Measurement of ozone and  
843 water vapor by Airbus in-service aircraft: The MOZAIC airborne program, an overview, *Journal*  
844 *of Geophysical Research: Atmospheres*, 103(D19), 25631–25642, doi:10.1029/98JD00977,  
845 1998.

846 Martin, B. D., Fuelberg, H. E., Blake, N. J., Crawford, J. H., Logan, J. A., Blake, D. R. and Sachse, G.  
847 W.: Long-range transport of Asian outflow to the equatorial Pacific, *Journal of Geophysical*  
848 *Research: Atmospheres*, 107(D2), PEM 5-1-PEM 5-18, doi:10.1029/2001JD001418, 2002.

849 Martín, M. V., Honrath, R. E., Owen, R. C., Pfister, G., Fialho, P. and Barata, F.: Significant  
850 enhancements of nitrogen oxides, black carbon, and ozone in the North Atlantic lower free  
851 troposphere resulting from North American boreal wildfires, *Journal of Geophysical Research:*  
852 *Atmospheres*, 111(D23), doi:10.1029/2006JD007530, 2006.

853 Mauzerall, D. L., Logan, J. A., Jacob, D. J., Anderson, B. E., Blake, D. R., Bradshaw, J. D., Heikes,  
854 B., Sachse, G. W., Singh, H. and Talbot, B.: Photochemistry in biomass burning plumes and  
855 implications for tropospheric ozone over the tropical South Atlantic, *Journal of Geophysical*  
856 *Research: Atmospheres*, 103(D7), 8401–8423, doi:10.1029/97JD02612, 1998.

857 Monks, P. S.: A review of the observations and origins of the spring ozone maximum,  
858 *Atmospheric Environment*, 34(21), 3545–3561, doi:10.1016/S1352-2310(00)00129-1, 2000.

859 Monks, P. S., Carpenter, L. J., Penkett, S. A., Ayers, G. P., Gillett, R. W., Galbally, I. E. and (Mick)  
860 Meyer, C. P.: Fundamental ozone photochemistry in the remote marine boundary layer: the  
861 soapex experiment, measurement and theory, *Atmospheric Environment*, 32(21), 3647–3664,  
862 doi:10.1016/S1352-2310(98)00084-3, 1998.

863 Monks, P. S., Salisbury, G., Holland, G., Penkett, S. A. and Ayers, G. P.: A seasonal comparison of  
864 ozone photochemistry in the remote marine boundary layer, *Atmospheric Environment*, 34(16),  
865 2547–2561, doi:10.1016/S1352-2310(99)00504-X, 2000.

866 Monks, P. S., Granier, C., Fuzzi, S., Stohl, A., Williams, M. L., Akimoto, H., Amann, M., Baklanov,  
867 A., Baltensperger, U., Bey, I., Blake, N., Blake, R. S., Carslaw, K., Cooper, O. R., Dentener, F.,  
868 Fowler, D., Fragkou, E., Frost, G. J., Generoso, S., Ginoux, P., Grewe, V., Guenther, A., Hansson,  
869 H. C., Henne, S., Hjorth, J., Hofzumahaus, A., Huntrieser, H., Isaksen, I. S. A., Jenkin, M. E.,  
870 Kaiser, J., Kanakidou, M., Klimont, Z., Kulmala, M., Laj, P., Lawrence, M. G., Lee, J. D., Liousse, C.,  
871 Maione, M., McFiggans, G., Metzger, A., Mieville, A., Moussiopoulos, N., Orlando, J. J., O'Dowd,  
872 C. D., Palmer, P. I., Parrish, D. D., Petzold, A., Platt, U., Pöschl, U., Prévôt, A. S. H., Reeves, C. E.,  
873 Reimann, S., Rudich, Y., Sellegri, K., Steinbrecher, R., Simpson, D., ten Brink, H., Theloke, J., van  
874 der Werf, G. R., Vautard, R., Vestreng, V., Vlachokostas, Ch. and von Glasow, R.: Atmospheric

875 composition change – global and regional air quality, *Atmospheric Environment*, 43(33), 5268–  
876 5350, doi:10.1016/j.atmosenv.2009.08.021, 2009.

877 Moxim, W. J. and Levy, H.: A model analysis of the tropical South Atlantic Ocean tropospheric  
878 ozone maximum: The interaction of transport and chemistry, *Journal of Geophysical Research:*  
879 *Atmospheres*, 105(D13), 17393–17415, doi:10.1029/2000JD900175, 2000.

880 Nath, D., Chen, W., Graf, H.-F., Lan, X., Gong, H., Nath, R., Hu, K. and Wang, L.: Subtropical  
881 Potential Vorticity Intrusion Drives Increasing Tropospheric Ozone over the Tropical Central  
882 Pacific, *Scientific Reports*, 6, 21370, doi:10.1038/srep21370, 2016.

883 Nédélec, P., Cammas, J.-P., Thouret, V., Athier, G., Cousin, J.-M., Legrand, C., Abonnel, C.,  
884 Lecoœur, F., Cayez, G. and Marizy, C.: An improved infrared carbon monoxide analyser for  
885 routine measurements aboard commercial Airbus aircraft: technical validation and first  
886 scientific results of the MOZAIC III programme, *Atmospheric Chemistry and Physics*, 3(5), 1551–  
887 1564, doi:https://doi.org/10.5194/acp-3-1551-2003, 2003.

888 Nédélec, P., Blot, R., Boulanger, D., Athier, G., Cousin, J.-M., Gautron, B., Petzold, A., Volz-  
889 Thomas, A. and Thouret, V.: Instrumentation on commercial aircraft for monitoring the  
890 atmospheric composition on a global scale: the IAGOS system, technical overview of ozone and  
891 carbon monoxide measurements, *Tellus B: Chemical and Physical Meteorology*, 68(s1), 27791,  
892 doi:10.3402/tellusb.v67.27791, 2015.

893 Neuman, J. A., Trainer, M., Aikin, K. C., Angevine, W. M., Brioude, J., Brown, S. S., de Gouw, J. A.,  
894 Dube, W. P., Flynn, J. H., Graus, M., Holloway, J. S., Lefer, B. L., Nedelec, P., Nowak, J. B., Parrish,  
895 D. D., Pollack, I. B., Roberts, J. M., Ryerson, T. B., Smit, H., Thouret, V. and Wagner, N. L.:  
896 Observations of ozone transport from the free troposphere to the Los Angeles basin, *Journal of*  
897 *Geophysical Research: Atmospheres*, 117(D21), n/a-n/a, doi:10.1029/2011JD016919, 2012.

898 Newell, R. E. and Evans, M. J.: Seasonal changes in pollutant transport to the North Pacific: The  
899 relative importance of Asian and European sources, *Geophysical Research Letters*, 27(16),  
900 2509–2512, doi:10.1029/2000GL011501, 2000.

901 Newton, R., Vaughan, G., Hints, E., Filus, M. T., Pan, L. L., Honomichl, S., Atlas, E., Andrews, S. J.  
902 and Carpenter, L. J.: Observations of ozone-poor air in the Tropical Tropopause Layer,  
903 *Atmospheric Chemistry and Physics Discussions*, 1–23, doi:10.5194/acp-2017-970, 2017.

904 Oltmans, S. J., Johnson, B. J., Harris, J. M., Vömel, H., Thompson, A. M., Koshy, K., Simon, P.,  
905 Bendura, R. J., Logan, J. A., Hasebe, F., Shiotani, M., Kirchhoff, V. W. J. H., Maata, M., Sami, G.,  
906 Samad, A., Tabuadravu, J., Enriquez, H., Agama, M., Cornejo, J. and Paredes, F.: Ozone in the  
907 Pacific tropical troposphere from ozonesonde observations, *Journal of Geophysical Research:*  
908 *Atmospheres*, 106(D23), 32503–32525, doi:10.1029/2000JD900834, 2001.

909 Oltmans, S. J., Lefohn, A. S., Shadwick, D., Harris, J. M., Scheel, H. E., Galbally, I., Tarasick, D. W.,  
910 Johnson, B. J., Brunke, E.-G., Claude, H., Zeng, G., Nichol, S., Schmidlin, F., Davies, J., Cuevas, E.,

911 Redondas, A., Naoe, H., Nakano, T. and Kawasato, T.: Recent tropospheric ozone changes – A  
 912 pattern dominated by slow or no growth, *Atmospheric Environment*, 67, 331–351,  
 913 doi:10.1016/j.atmosenv.2012.10.057, 2013.

914 Owen, R. C., Cooper, O. R., Stohl, A. and Honrath, R. E.: An analysis of the mechanisms of North  
 915 American pollutant transport to the central North Atlantic lower free troposphere, *Journal of*  
 916 *Geophysical Research: Atmospheres*, 111(D23), doi:10.1029/2006JD007062, 2006.

917 Pan, L. L., Honomichl, S. B., Randel, W. J., Apel, E. C., Atlas, E. L., Beaton, S. P., Bresch, J. F.,  
 918 Hornbrook, R., Kinnison, D. E., Lamarque, J.-F., Saiz-Lopez, A., Salawitch, R. J. and Weinheimer,  
 919 A. J.: Bimodal distribution of free tropospheric ozone over the tropical western Pacific revealed  
 920 by airborne observations, *Geophysical Research Letters*, 42(18), 7844–7851,  
 921 doi:10.1002/2015GL065562, 2015.

922 Parrish, D. D., Galbally, I. E., Lamarque, J. -F., Naik, V., Horowitz, Shindell, D. T., Oltmans, S. J.,  
 923 Derwent, R., Tanimoto, H., Labuschagne, C. and Cupeiro, M.: Seasonal cycles of O<sub>3</sub> in the  
 924 marine boundary layer: Observation and model simulation comparisons, *Journal of Geophysical*  
 925 *Research: Atmospheres*, 121(1), 538–557, doi:10.1002/2015JD024101, 2016.

926 Parrish, D. D., Derwent, R. G., Steinbrecht, W., Stübi, R., Malderen, R. V., Steinbacher, M., Trickl,  
 927 T., Ries, L. and Xu, X.: Zonal Similarity of Long-term Changes and Seasonal Cycles of Baseline  
 928 Ozone at Northern Mid-latitudes, *Journal of Geophysical Research: Atmospheres*, n/a(n/a),  
 929 e2019JD031908, doi:10.1029/2019JD031908, 2020.

930 Perkins, S. E., Pitman, A. J., Holbrook, N. J. and McAneney, J.: Evaluation of the AR4 Climate  
 931 Models' Simulated Daily Maximum Temperature, Minimum Temperature, and Precipitation  
 932 over Australia Using Probability Density Functions, *J. Climate*, 20(17), 4356–4376,  
 933 doi:10.1175/JCLI4253.1, 2007.

934 Petetin, H., Thouret, V., Fontaine, A., Sauvage, B., Athier, G., Blot, R., Boulanger, D., Cousin, J.-  
 935 M. and Nédélec, P.: Characterising tropospheric O<sub>3</sub> and CO around Frankfurt over the period  
 936 1994–2012 based on MOZAIC–IAGOS aircraft measurements, *Atmos. Chem. Phys.*, 16(23),  
 937 15147–15163, doi:10.5194/acp-16-15147-2016, 2016.

938 Petzold, A., Thouret, V., Gerbig, C., Zahn, A., Brenninkmeijer, C. A. M., Gallagher, M., Hermann,  
 939 M., Pontaud, M., Ziereis, H., Boulanger, D., Marshall, J., Nédélec, P., Smit, H. G. J., Friess, U.,  
 940 Flaud, J.-M., Wahner, A., Cammas, J.-P., Volz-Thomas, A. and TEAM, I.: Global-scale atmosphere  
 941 monitoring by in-service aircraft – current achievements and future prospects of the European  
 942 Research Infrastructure IAGOS, *Tellus B: Chemical and Physical Meteorology*, 67(1), 28452,  
 943 doi:10.3402/tellusb.v67.28452, 2015.

944 Pickering, K. E., Thompson, A. M., Wang, Y., Tao, W.-K., McNamara, D. P., Kirchhoff, V. W. J. H.,  
 945 Heikes, B. G., Sachse, G. W., Bradshaw, J. D., Gregory, G. L. and Blake, D. R.: Convective  
 946 transport of biomass burning emissions over Brazil during TRACE A, *Journal of Geophysical*  
 947 *Research: Atmospheres*, 101(D19), 23993–24012, doi:10.1029/96JD00346, 1996.

948 Prather, M. J., Zhu, X., Flynn, C. M., Strode, S. A., Rodriguez, J. M., Steenrod, S. D., Liu, J.,  
 949 Lamarque, J.-F., Fiore, A. M., Horowitz, L. W., Mao, J., Murray, L. T., Shindell, D. T. and Wofsy, S.  
 950 C.: Global atmospheric chemistry – which air matters, *Atmospheric Chemistry and Physics*,  
 951 17(14), 9081–9102, doi:<https://doi.org/10.5194/acp-17-9081-2017>, 2017.

952 Proffitt, M. H. and McLaughlin, R. J.: Fast-response dual-beam UV-absorption ozone  
 953 photometer suitable for use on stratospheric balloons, *Review of Scientific Instruments*, 54(12),  
 954 1719–1728, doi:10.1063/1.1137316, 1983.

955 Ridley, B. A., Grahek, F. E. and Walega, J. G.: A Small High-Sensitivity, Medium-Response Ozone  
 956 Detector Suitable for Measurements from Light Aircraft, *J. Atmos. Oceanic Technol.*, 9(2), 142–  
 957 148, doi:10.1175/1520-0426(1992)009<0142:ASHSMR>2.0.CO;2, 1992.

958 Santoni, G. W., Daube, B. C., Kort, E. A., Jiménez, R., Park, S., Pittman, J. V., Gottlieb, E., Xiang,  
 959 B., Zahniser, M. S., Nelson, D. D., McManus, J. B., Peischl, J., Ryerson, T. B., Holloway, J. S.,  
 960 Andrews, A. E., Sweeney, C., Hall, B., Hints, E. J., Moore, F. L., Elkins, J. W., Hurst, D. F.,  
 961 Stephens, B. B., Bent, J. and Wofsy, S. C.: Evaluation of the airborne quantum cascade laser  
 962 spectrometer (QCLS) measurements of the carbon and greenhouse gas suite &ndash; CO<sub>2</sub>, CH<sub>4</sub>,  
 963 N<sub>2</sub>O, and CO &ndash; during the CalNex and HIPPO campaigns, *Atmospheric Measurement*  
 964 *Techniques*, 7(6), 1509–1526, doi:<https://doi.org/10.5194/amt-7-1509-2014>, 2014.

965 Sauvage, B., Thouret, V., Thompson, A. M., Witte, J. C., Cammas, J.-P., Nédélec, P. and Athier,  
 966 G.: Enhanced view of the “tropical Atlantic ozone paradox” and “zonal wave one” from the in  
 967 situ MOZAIC and SHADOZ data, *Journal of Geophysical Research: Atmospheres*, 111(D1),  
 968 doi:10.1029/2005JD006241, 2006.

969 Schultz, M. G., Jacob, D. J., Wang, Y., Logan, J. A., Atlas, E. L., Blake, D. R., Blake, N. J., Bradshaw,  
 970 J. D., Browell, E. V., Fenn, M. A., Flocke, F., Gregory, G. L., Heikes, B. G., Sachse, G. W.,  
 971 Sandholm, S. T., Shetter, R. E., Singh, H. B. and Talbot, R. W.: On the origin of tropospheric  
 972 ozone and NO<sub>x</sub> over the tropical South Pacific, *Journal of Geophysical Research: Atmospheres*,  
 973 104(D5), 5829–5843, doi:10.1029/98JD02309, 1999.

974 Shen, Z., Liu, J., Horowitz, L. W., Henze, D. K., Fan, S., H., L. I., Mauzerall, D. L., Lin, J.-T. and Tao,  
 975 S.: Analysis of transpacific transport of black carbon during HIPPO-3: implications for black  
 976 carbon aging, *Atmospheric Chemistry and Physics*, 14(12), 6315–6327, doi:10.5194/acp-14-  
 977 6315-2014, 2014.

978 Shindell, D., Kuylensstierna, J. C. I., Vignati, E., Dingenen, R. van, Amann, M., Klimont, Z.,  
 979 Anenberg, S. C., Muller, N., Janssens-Maenhout, G., Raes, F., Schwartz, J., Faluvegi, G., Pozzoli,  
 980 L., Kupiainen, K., Höglund-Isaksson, L., Emberson, L., Streets, D., Ramanathan, V., Hicks, K.,  
 981 Oanh, N. T. K., Milly, G., Williams, M., Demkine, V. and Fowler, D.: Simultaneously Mitigating  
 982 Near-Term Climate Change and Improving Human Health and Food Security, *Science*,  
 983 335(6065), 183–189, doi:10.1126/science.1210026, 2012.

984 Singh, H. B., Herlth, D., Kolyer, R., Chatfield, R., Viezee, W., Salas, L. J., Chen, Y., Bradshaw, J. D.,  
985 Sandholm, S. T., Talbot, R., Gregory, G. L., Anderson, B., Sachse, G. W., Browell, E., Bachmeier,  
986 A. S., Blake, D. R., Heikes, B., Jacob, D. and Fuelberg, H. E.: Impact of biomass burning emissions  
987 on the composition of the South Atlantic troposphere: Reactive nitrogen and ozone, *Journal of*  
988 *Geophysical Research: Atmospheres*, 101(D19), 24203–24219, doi:10.1029/96JD01018, 1996a.

989 Singh, H. B., Gregory, G. L., Anderson, B., Browell, E., Sachse, G. W., Davis, D. D., Crawford, J.,  
990 Bradshaw, J. D., Talbot, R., Blake, D. R., Thornton, D., Newell, R. and Merrill, J.: Low ozone in the  
991 marine boundary layer of the tropical Pacific Ocean: Photochemical loss, chlorine atoms, and  
992 entrainment, *Journal of Geophysical Research: Atmospheres*, 101(D1), 1907–1917,  
993 doi:10.1029/95JD01028, 1996b.

994 Singh, H. B., Herlth, D., Kolyer, R., Salas, L., Bradshaw, J. D., Sandholm, S. T., Davis, D. D.,  
995 Crawford, J., Kondo, Y., Koike, M., Talbot, R., Gregory, G. L., Sachse, G. W., Browell, E., Blake, D.  
996 R., Rowland, F. S., Newell, R., Merrill, J., Heikes, B., Liu, S. C., Crutzen, P. J. and Kanakidou, M.:  
997 Reactive nitrogen and ozone over the western Pacific: Distribution, partitioning, and sources, *J.*  
998 *Geophys. Res.*, 101(D1), 1793–1808, doi:10.1029/95JD01029, 1996c.

999 Solomon, S., Thompson, D. W. J., Portmann, R. W., Oltmans, S. J. and Thompson, A. M.: On the  
1000 distribution and variability of ozone in the tropical upper troposphere: Implications for tropical  
1001 deep convection and chemical-dynamical coupling, *Geophysical Research Letters*, 32(23),  
1002 doi:10.1029/2005GL024323, 2005.

1003 Stauffer, R. M., Thompson, A. M. and Witte, J. C.: Characterizing Global Ozone Profile  
1004 Variability From Surface to the UT/LS With a Clustering Technique and MERRA-2 Reanalysis,  
1005 *Journal of Geophysical Research: Atmospheres*, 123(11), 6213–6229,  
1006 doi:10.1029/2018JD028465, 2018.

1007 Stedman, D. H., Daby, E. E., Stuhl, F. and Niki, H.: Analysis of Ozone and Nitric Oxide by a  
1008 Chemiluminescent Method in Laboratory and Atmospheric Studies of Photochemical Smog,  
1009 *Journal of the Air Pollution Control Association*, 22(4), 260–263,  
1010 doi:10.1080/00022470.1972.10469635, 1972.

1011 Tarasick, D. W. and Bottenheim, J. W.: Surface ozone depletion episodes in the Arctic and  
1012 Antarctic from historical ozonesonde records, *Atmospheric Chemistry and Physics*, 2(3), 197–  
1013 205, doi:https://doi.org/10.5194/acp-2-197-2002, 2002.

1014 Tarasick, D. W., Carey-Smith, T. K., Hocking, W. K., Moeini, O., He, H., Liu, J., Osman, M. K.,  
1015 Thompson, A. M., Johnson, B. J., Oltmans, S. J. and Merrill, J. T.: Quantifying stratosphere-  
1016 troposphere transport of ozone using balloon-borne ozonesondes, radar windprofilers and  
1017 trajectory models, *Atmospheric Environment*, 198, 496–509,  
1018 doi:10.1016/j.atmosenv.2018.10.040, 2019b.

1019 Tarasick, D. W., Galbally, I. E., Cooper, O. R., Schultz, M. G., Ancellet, G., Leblanc, T., Wallington,  
1020 T. J., Ziemke, J., Liu, X., Steinbacher, M., Staehelin, J., Vigouroux, C., Hannigan, J. W., García, O.,



- 1021 Foret, G., Zanis, P., Weatherhead, E., Petropavlovskikh, I., Worden, H., Osman, M., Liu, J.,  
1022 Chang, K.-L., Gaudel, A., Lin, M., Granados-Muñoz, M., Thompson, A. M., Oltmans, S. J., Cuesta,  
1023 J., Dufour, G., Thouret, V., Hassler, B., Trickl, T. and Neu, J. L.: Tropospheric Ozone Assessment  
1024 Report: Tropospheric ozone from 1877 to 2016, observed levels, trends and uncertainties, *Elem*  
1025 *Sci Anth*, 7(1), 39, doi:10.1525/elementa.376, 2019a.
- 1026 Thompson, A. M., Johnson, J. E., Torres, A. L., Bates, T. S., Kelly, K. C., Atlas, E., Greenberg, J. P.,  
1027 Donahue, N. M., Yvon, S. A., Saltzman, E. S., Heikes, B. G., Mosher, B. W., Shashkov, A. A. and  
1028 Yegorov, V. I.: Ozone observations and a model of marine boundary layer photochemistry  
1029 during SAGA 3, *Journal of Geophysical Research: Atmospheres*, 98(D9), 16955–16968,  
1030 doi:10.1029/93JD00258, 1993.
- 1031 Thompson, A. M., Pickering, K. E., McNamara, D. P., Schoeberl, M. R., Hudson, R. D., Kim, J. H.,  
1032 Browell, E. V., Kirchhoff, V. W. J. H. and Nganga, D.: Where did tropospheric ozone over  
1033 southern Africa and the tropical Atlantic come from in October 1992? Insights from TOMS, GTE  
1034 TRACE A, and SAFARI 1992, *Journal of Geophysical Research: Atmospheres*, 101(D19), 24251–  
1035 24278, doi:10.1029/96JD01463, 1996.
- 1036 Thompson, A. M., Doddridge, B. G., Witte, J. C., Hudson, R. D., Luke, W. T., Johnson, J. E.,  
1037 Johnson, B. J., Oltmans, S. J. and Weller, R.: A tropical Atlantic Paradox: Shipboard and satellite  
1038 views of a tropospheric ozone maximum and wave-one in January–February 1999, *Geophysical*  
1039 *Research Letters*, 27(20), 3317–3320, doi:10.1029/1999GL011273, 2000.
- 1040 Thompson, A. M., Miller, S. K., Tilmes, S., Kollonige, D. W., Witte, J. C., Oltmans, S. J., Johnson,  
1041 B. J., Fujiwara, M., Schmidlin, F. J., Coetzee, G. J. R., Komala, N., Maata, M., Mohamad, M. B.,  
1042 Nguyo, J., Mutai, C., Ogino, S. Y., Silva, F. R. D., Leme, N. M. P., Posny, F., Scheele, R., Selkirk, H.  
1043 B., Shiotani, M., Stbi, R., Levrat, G., Calpini, B., Thouret, V., Tsuruta, H., Canossa, J. V., Vmel, H.,  
1044 Yonemura, S., Diaz, J. A., Thanh, N. T. T. and Ha, H. T. T.: Southern Hemisphere Additional  
1045 Ozonesondes (SHADOZ) ozone climatology (2005-2009): Tropospheric and tropical tropopause  
1046 layer (TTL) profiles with comparisons to OMI-based ozone products, *Journal of Geophysical*  
1047 *Research Atmospheres*, 117(23), D23301, doi:10.1029/2011JD016911, 2012.
- 1048 Thompson, A. M., Witte, J. C., Sterling, C., Jordan, A., Johnson, B. J., Oltmans, S. J., Fujiwara, M.,  
1049 Vömel, H., Allaart, M., PETERS, A., Coetzee, G. J. R., Posny, F., Corrales, E., Diaz, J. A., Félix, C.,  
1050 Komala, N., Lai, N., Ahn Nguyen, H. T., Maata, M., Mani, F., Zainal, Z., Ogino, S., Paredes, F.,  
1051 Penha, T. L. B., da Silva, F. R., Sallons-Mitro, S., Selkirk, H. B., Schmidlin, F. J., Stübi, R. and  
1052 Thiongo, K.: First Reprocessing of Southern Hemisphere Additional Ozonesondes (SHADOZ)  
1053 Ozone Profiles (1998-2016): 2. Comparisons With Satellites and Ground-Based Instruments:  
1054 SHADOZ Data Evaluation, *Journal of Geophysical Research: Atmospheres*,  
1055 doi:10.1002/2017JD027406, 2017.
- 1056 Thompson, A. M., Smit, H. G. J., Witte, J. C., Stauffer, R. M., Johnson, B. J., Morris, G., von der  
1057 Gathen, P., Van Malderen, R., Davies, J., PETERS, A., Allaart, M., Posny, F., Kivi, R., Cullis, P., Hoang  
1058 Anh, N. T., Corrales, E., Machinini, T., da Silva, F. R., Paiman, G., Thiong'o, K., Zainal, Z., Brothers,  
1059 G. B., Wolff, K. R., Nakano, T., Stübi, R., Romanens, G., Coetzee, G. J. R., Diaz, J. A., Mitro, S.,

- 1060 Mohamad, M. and Ogino, S.-Y.: Ozone-sonde Quality Assurance: The JOSIE–SHADOZ (2017)  
1061 Experience, *Bull. Amer. Meteor. Soc.*, 100(1), 155–171, doi:10.1175/BAMS-D-17-0311.1, 2019.
- 1062 Thompson, C. R., Ryerson, T. B., Peischl, J., Barletta, B., Blake, D. R., Butler, A. H., Crounse, J. D.,  
1063 Evans, M. J., Fisher, J. A., Huey, L. G., Kim, M. J., Laubach, A., Moore, F. L., Ray, E. A., Murray, L.  
1064 T., Sherwen, T., Strode, S. A., Wennberg, P. O. and Yu, P.: Global-scale Airborne Observations of  
1065 Tropospheric Reactive Nitrogen Species from the NASA Atmospheric Tomography Mission, AGU  
1066 Fall Meeting Abstracts, 14 [online] Available from:  
1067 <http://adsabs.harvard.edu/abs/2017AGUFM.A14D..02T> (Accessed 16 March 2020b), 2017.
- 1068 Thouret, V., Marenco, A., Logan, J. A., Nédélec, P. and Grouhel, C.: Comparisons of ozone  
1069 measurements from the MOZAIC airborne program and the ozone sounding network at eight  
1070 locations, *Journal of Geophysical Research: Atmospheres*, 103(D19), 25695–25720,  
1071 doi:10.1029/98JD02243, 1998.
- 1072 Tilmes, S., Lamarque, J.-F., Emmons, L. K., Conley, A., Schultz, M. G., Saunio, M., Thouret, V.,  
1073 Thompson, A. M., Oltmans, S. J., Johnson, B. and Tarasick, D.: Technical Note: Ozone-sonde  
1074 climatology between 1995 and 2011: description, evaluation and applications, *Atmospheric  
1075 Chemistry and Physics*, 12(16), 7475–7497, doi:<https://doi.org/10.5194/acp-12-7475-2012>,  
1076 2012.
- 1077 Trickl, T., Cooper, O. R., Eisele, H., James, P., Mücke, R. and Stohl, A.: Intercontinental transport  
1078 and its influence on the ozone concentrations over central Europe: Three case studies, *Journal  
1079 of Geophysical Research: Atmospheres*, 108(D12), doi:10.1029/2002JD002735, 2003.
- 1080 Wespes, C., Hurtmans D., Clerbaux C. and Coheur P.-F.: O<sub>3</sub> variability in the troposphere as  
1081 observed by IASI over 2008–2016: Contribution of atmospheric chemistry and dynamics,  
1082 *Journal of Geophysical Research: Atmospheres*, 122(4), 2429–2451,  
1083 doi:10.1002/2016JD025875, 2017.
- 1084 Williams, J. E., Scheele, M. P., van Velthoven, P. F. J., Thouret, V., Saunio, M., Reeves, C. E. and  
1085 Cammas, J.-P.: The influence of biomass burning and transport on tropospheric composition  
1086 over the tropical Atlantic Ocean and Equatorial Africa during the West African monsoon in  
1087 2006, *Atmospheric Chemistry and Physics*, 10(20), 9797–9817, doi:10.5194/acp-10-9797-2010,  
1088 2010.
- 1089 Witte, J. C., Thompson, A. M., Smit, H. G. J., Vömel, H., Posny, F. and Stübi, R.: First  
1090 Reprocessing of Southern Hemisphere ADditional OZone-sondes Profile Records: 3. Uncertainty  
1091 in Ozone Profile and Total Column, *Journal of Geophysical Research: Atmospheres*, 123(6),  
1092 3243–3268, doi:10.1002/2017JD027791, 2018.
- 1093 Wofsy, S. C.: HIPER Pole-to-Pole Observations (HIPPO): fine-grained, global-scale  
1094 measurements of climatically important atmospheric gases and aerosols, *Philosophical  
1095 Transactions of the Royal Society A: Mathematical, Physical and Engineering Sciences*,  
1096 369(1943), 2073–2086, doi:10.1098/rsta.2010.0313, 2011.

- 1097 Young, P. J., Archibald, A. T., Bowman, K. W., Lamarque, J.-F., Naik, V., Stevenson, D. S., Tilmes,  
1098 S., Voulgarakis, A., Wild, O., Bergmann, D., Cameron-Smith, P., Cionni, I., Collins, W. J., Dalsøren,  
1099 S. B., Doherty, R. M., Eyring, V., Faluvegi, G., Horowitz, L. W., Josse, B., Lee, Y. H., MacKenzie, I.  
1100 A., Nagashima, T., Plummer, D. A., Righi, M., Rumbold, S. T., Skeie, R. B., Shindell, D. T., Strode,  
1101 S. A., Sudo, K., Szopa, S. and Zeng, G.: Pre-industrial to end 21st century projections of  
1102 tropospheric ozone from the Atmospheric Chemistry and Climate Model Intercomparison  
1103 Project (ACCMIP), *Atmos. Chem. Phys.*, 13(4), 2063–2090, doi:10.5194/acp-13-2063-2013,  
1104 2013.
- 1105 Young, P. J., Naik, V., Fiore, A. M., Gaudel, A., Guo, J., Lin, M. Y., Neu, J. L., Parrish, D. D., Rieder,  
1106 H. E., Schnell, J. L., Tilmes, S., Wild, O., Zhang, L., Ziemke, J. R., Brandt, J., Delcloo, A., Doherty, R.  
1107 M., Geels, C., Hegglin, M. I., Hu, L., Im, U., Kumar, R., Luhar, A., Murray, L., Plummer, D.,  
1108 Rodriguez, J., Saiz-Lopez, A., Schultz, M. G., Woodhouse, M. T. and Zeng, G.: Tropospheric  
1109 Ozone Assessment Report: Assessment of global-scale model performance for global and  
1110 regional ozone distributions, variability, and trends, *Elem Sci Anth*, 6(1),  
1111 doi:10.1525/elementa.265, 2018.
- 1112 Zbinden, R. M., Thouret, V., Ricaud, P., Carminati, F., Cammas, J.-P. and Nédélec, P.: Climatology  
1113 of pure tropospheric profiles and column contents of ozone and carbon monoxide using  
1114 MOZAIC in the mid-northern latitudes (24° N to 50° N) from 1994 to 2009, *Atmospheric  
1115 Chemistry and Physics*, 13(24), 12363–12388, doi:https://doi.org/10.5194/acp-13-12363-2013,  
1116 2013.
- 1117 Zhang, B., Owen, R. C., Perlinger, J. A., Helmig, D., Martín, M. V., Kramer, L., Mazzoleni, L. R. and  
1118 Mazzoleni, C.: Ten-year chemical signatures associated with long-range transport observed in  
1119 the free troposphere over the central North Atlantic, *Elem Sci Anth*, 5(0),  
1120 doi:10.1525/elementa.194, 2017.
- 1121 Zhang, L., Jacob, D. J., Boersma, K. F., Jaffe, D. A., Olson, J. R., Bowman, K. W., Worden, J. R.,  
1122 Thompson, A. M., Avery, M. A., Cohen, R. C., Dibb, J. E., Flock, F. M., Fuelberg, H. E., Huey, L. G.,  
1123 McMillan, W. W., Singh, H. B. and Weinheimer, A. J.: Transpacific transport of ozone pollution  
1124 and the effect of recent Asian emission increases on air quality in North America: an integrated  
1125 analysis using satellite, aircraft, ozonesonde, and surface observations, *Atmospheric Chemistry  
1126 and Physics*, 8(20), 6117–6136, doi:https://doi.org/10.5194/acp-8-6117-2008, 2008.
- 1127 Ziemke, J. R., Chandra S. and Bhartia P. K.: A 25-year data record of atmospheric ozone in the  
1128 Pacific from Total Ozone Mapping Spectrometer (TOMS) cloud slicing: Implications for ozone  
1129 trends in the stratosphere and troposphere, *Journal of Geophysical Research: Atmospheres*,  
1130 110(D15), doi:10.1029/2004JD005687, 2005.
- 1131 Ziemke, J. R., Chandra S., Duncan B. N., Froidevaux L., Bhartia P. K., Levelt P. F. and Waters J.  
1132 W.: Tropospheric ozone determined from Aura OMI and MLS: Evaluation of measurements and  
1133 comparison with the Global Modeling Initiative's Chemical Transport Model, *Journal of  
1134 Geophysical Research: Atmospheres*, 111(D19), doi:10.1029/2006JD007089, 2006.

1135 Ziemke, J. R., Strode, S. A., Douglass, A. R., Joiner, J., Vasilkov, A., Oman, L. D., Liu, J., Strahan, S.  
1136 E., Bhartia, P. K. and Haffner, D. P.: A cloud-ozone data product from Aura OMI and MLS  
1137 satellite measurements, *Atmos. Meas. Tech.*, 10(11), 4067–4078, doi:10.5194/amt-10-4067-  
1138 2017, 2017.

1139

1140

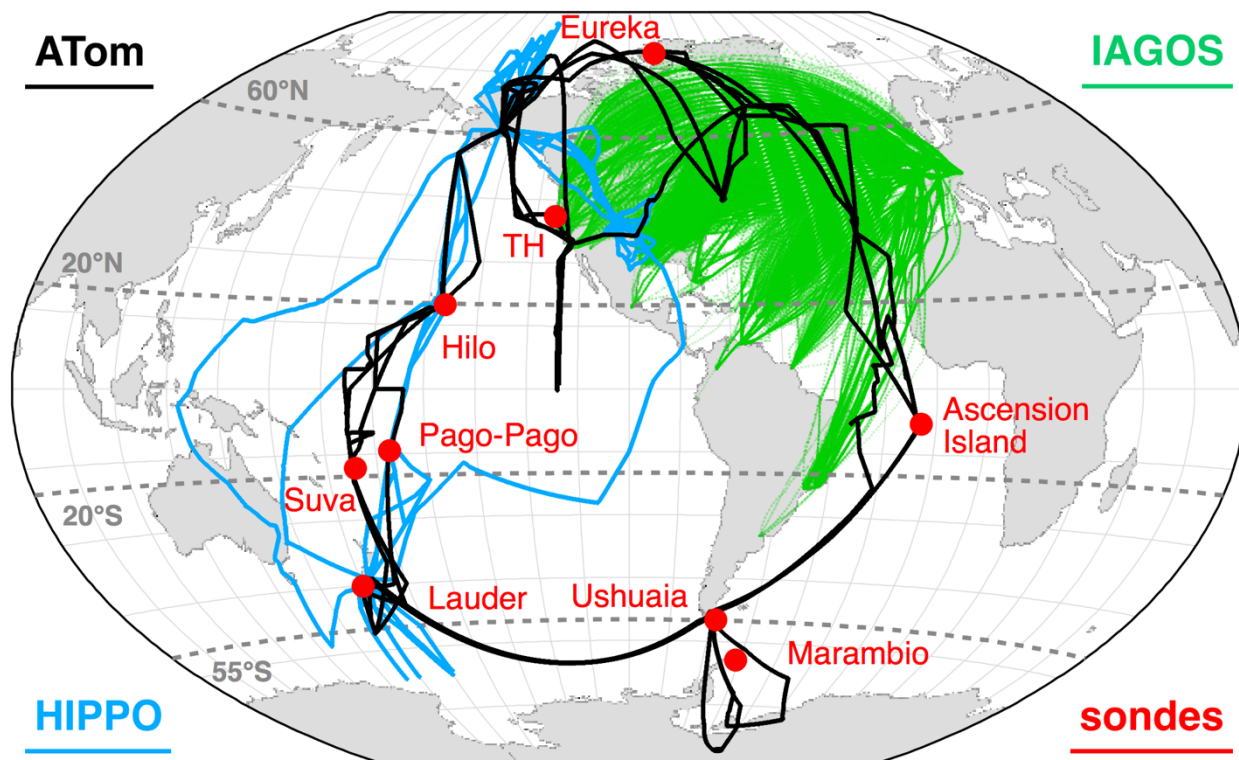


**Figure 1** The location and flight tracks of all O<sub>3</sub> monitoring platforms used in this work are illustrated with different markers and colors. The ATom flight track is in black, the HIPPO flight track is in blue, IAGOS flight paths are in green, and the ozonesonde launching sites are indicated by the red markers. The dotted grey lines define the latitudinal bands over which individual ATom and HIPPO profiles were averaged to derive a regional O<sub>3</sub> distribution: the tropics (20° S – 20° N), the midlatitudes (55° S – 20° S; 20° N – 60° N), and the high-latitudes (90° S – 55° S; 60° N – 90° N). Only data from remote oceanic flight segments of ATom and HIPPO missions were used in this work.

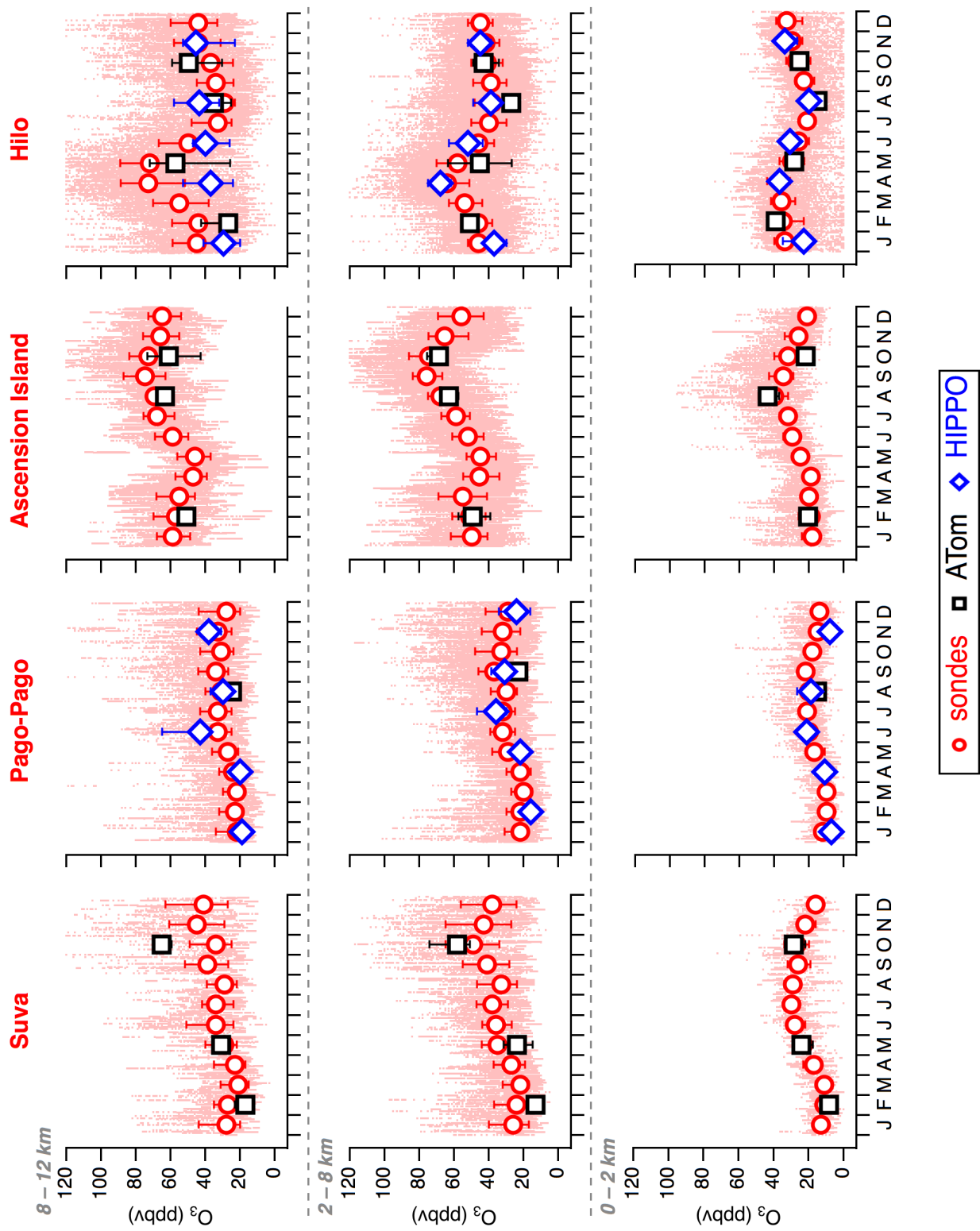


**Figure 2** Comparison of ATom (black squares) and HIPPO (blue diamonds) monthly median O<sub>3</sub> with ozonesonde (red circles) records from the four tropical sites. Markers indicate the median and the bars indicate the 25<sup>th</sup> and 75<sup>th</sup> percentiles. The three rows, from bottom to top, correspond to the boundary layer (0–2 km), the free troposphere (2–8 km), and the UTLS (8–12 km). The pink dots show every O<sub>3</sub> data point measured by ozonesondes for the timeframes indicated in Table S2.

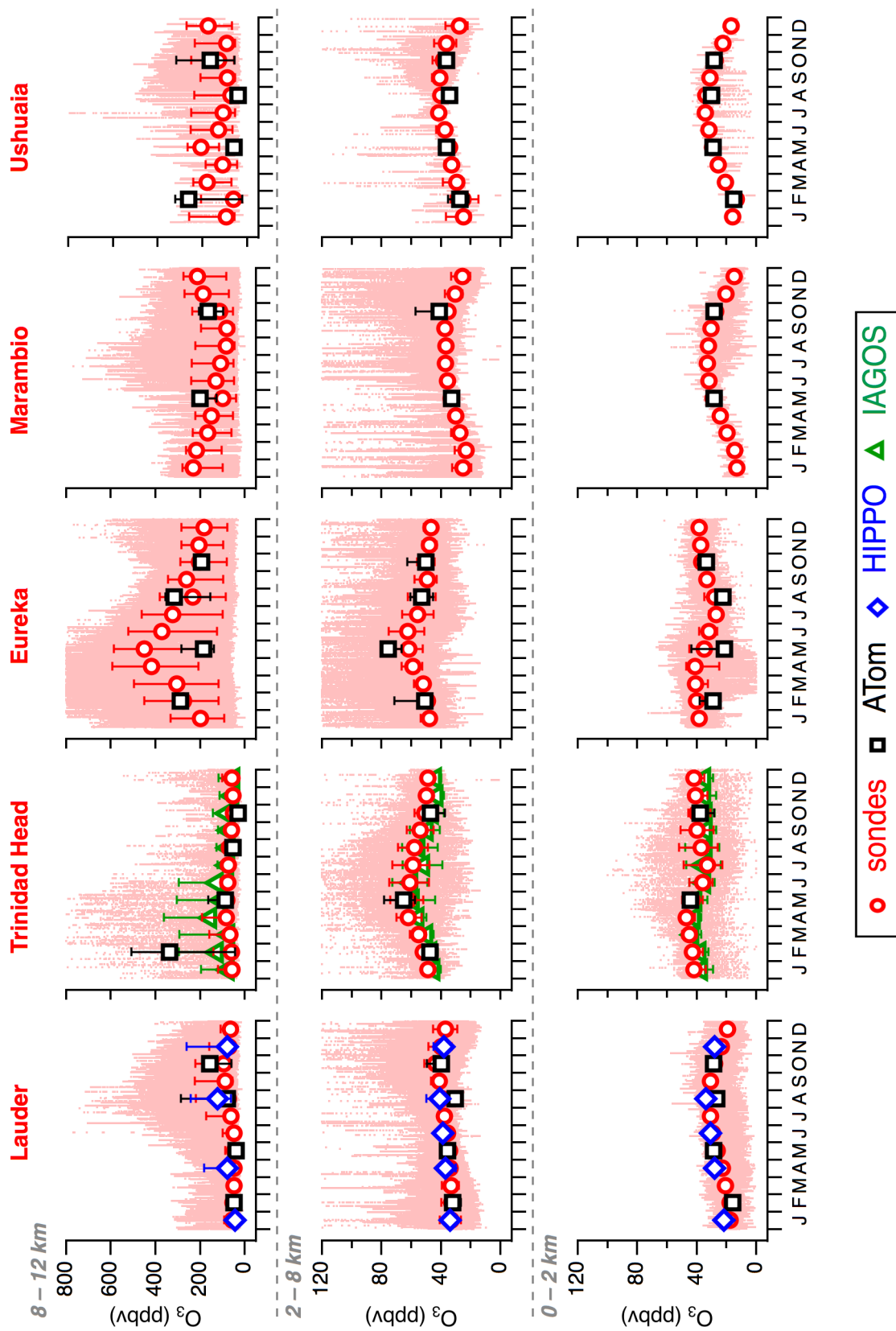




**Figure 3** Same as in Figure 2 but for ozonesonde launching sites located in the middle- and high-latitudes. O<sub>3</sub> data obtained from the IAGOS program (green triangles) during descents into San Francisco Bay-area airports were also added to the Trinidad Head site for comparison.

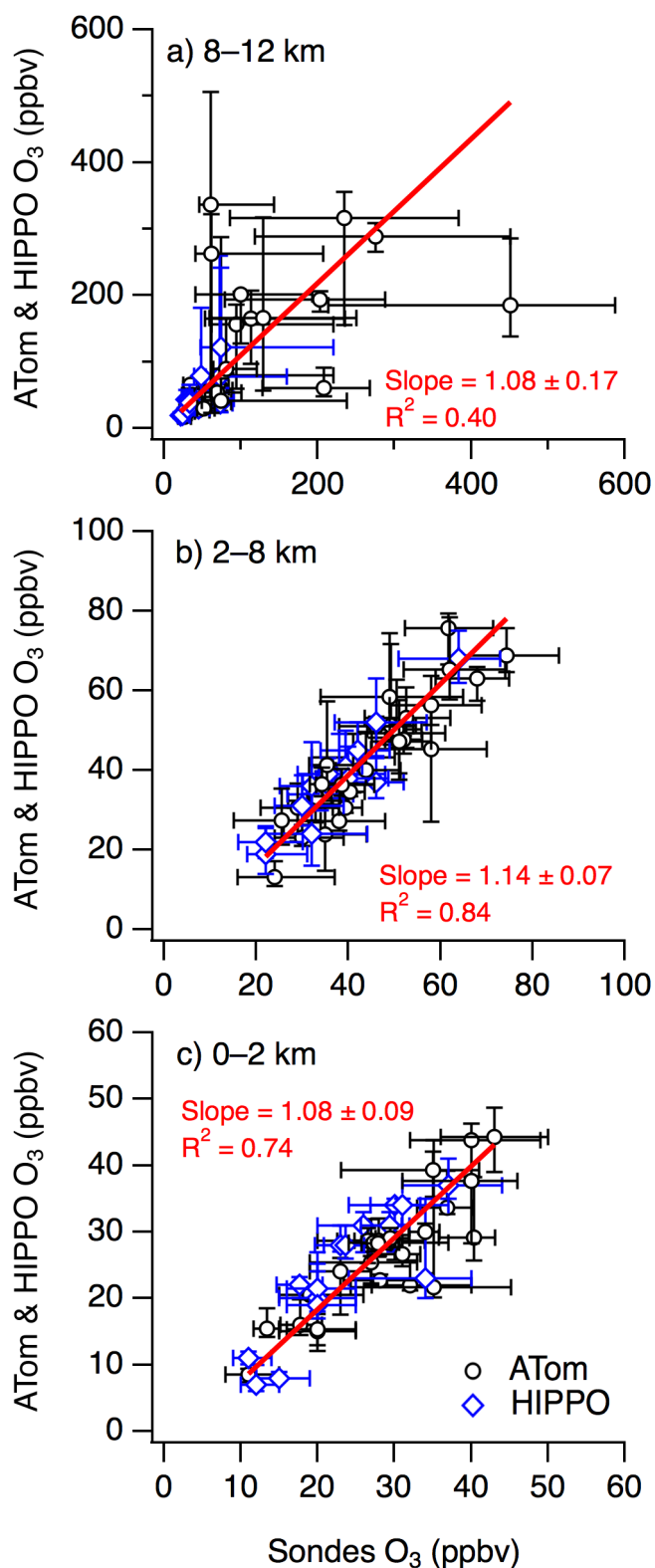


**Figure 4** ATom (black circles) and HIPPO (blue diamonds) combined monthly median O<sub>3</sub> vs. monthly median O<sub>3</sub> from ozonesondes at the nine sites considered in this study. The three panels

indicate the correlations for a) the UTLS (8–12 km), b) the free troposphere (2–8 km), and c) the boundary layer (0–2 km). The orthogonal regression fits are two-sided but not weighted.

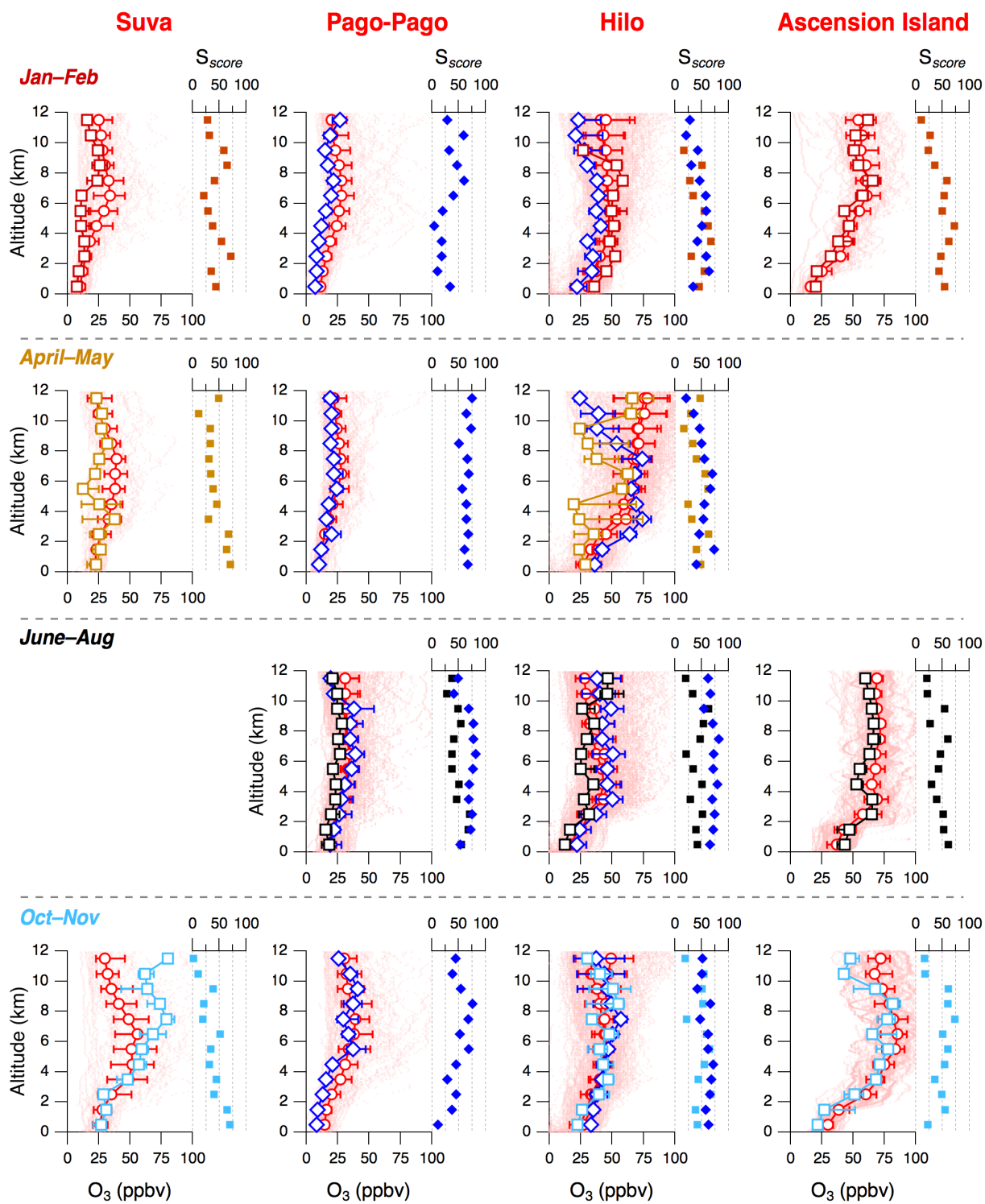


**Figure 5** Seasonal comparison of 1 km-vertically-binned ATom (colored squares) and HIPPO (blue diamonds) median  $O_3$  with ozonesonde (red circles) records at four sites in the tropics (Suva in Fiji, Pago-Pago in American Samoa, Hilo in Hawaii, and Ascension Island). Markers indicate the median and the bars are the 25<sup>th</sup> and 75<sup>th</sup> percentiles. The  $S_{score}$  is a metric of how well ATom

and HIPPO 1 km-binned  $O_3$  probability distribution functions (PDFs) overlap with the corresponding 1 km-binned  $O_3$  PDFs from ozonesondes. The  $S_{score}$  shown with squares compares ATom with ozonesondes, and the  $S_{score}$  shown with blue diamonds compares HIPPO with ozonesondes. The pink dots show every  $O_3$  data point measured by ozonesondes for the timeframes indicated in Table S2.

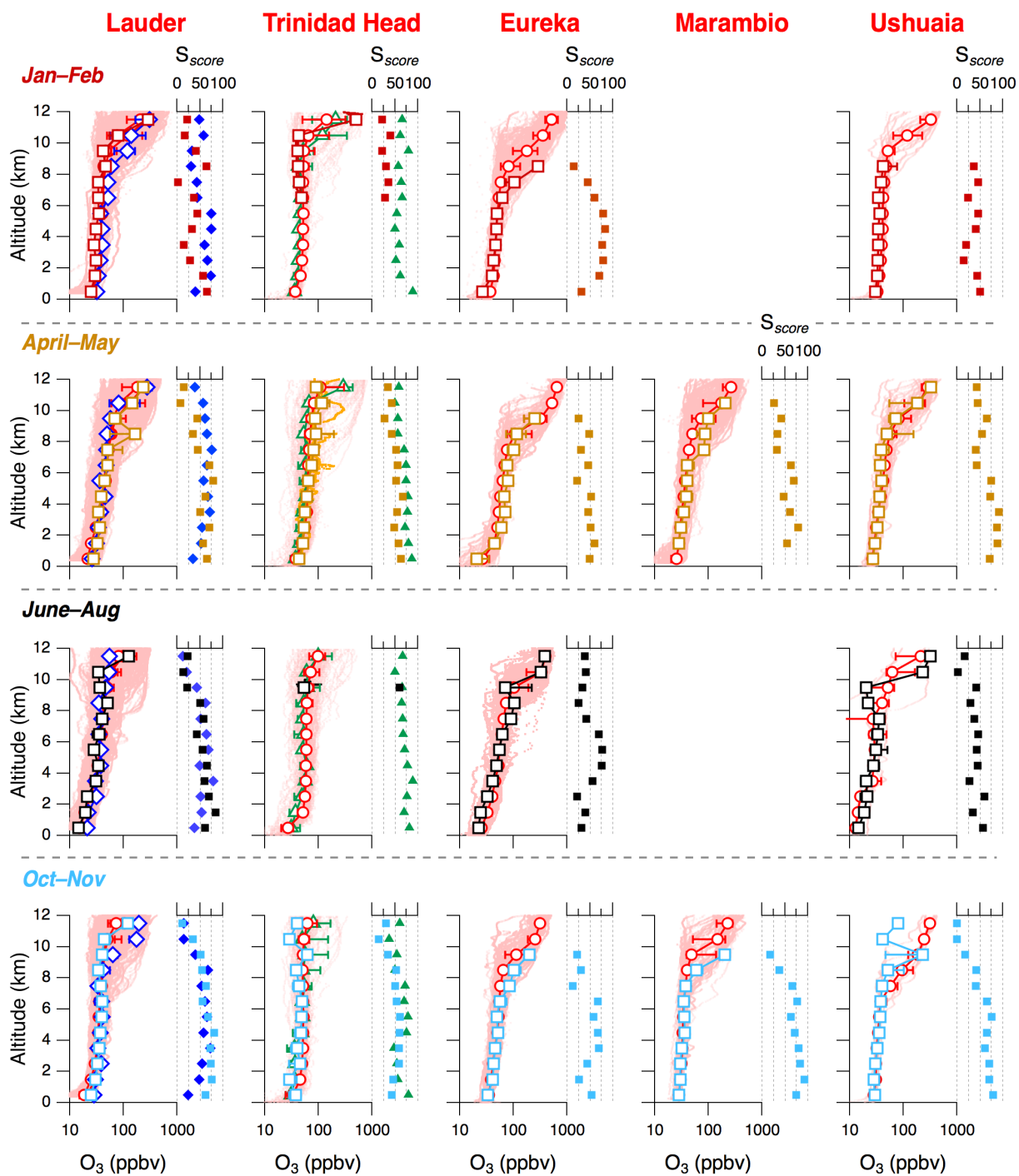


**Figure 6** Same as in Figure 5 but for ozonesonde launching sites located in middle- and high-latitudes (Lauder in New Zealand, Trinidad Head in the USA, Eureka in Canada, Ushuaia in Argentina, and Marambio in Antarctica).  $O_3$  data obtained from the IAGOS program (green triangles) during descents into San Francisco Bay-area nearby airports were also added to the Trinidad Head site for comparison.

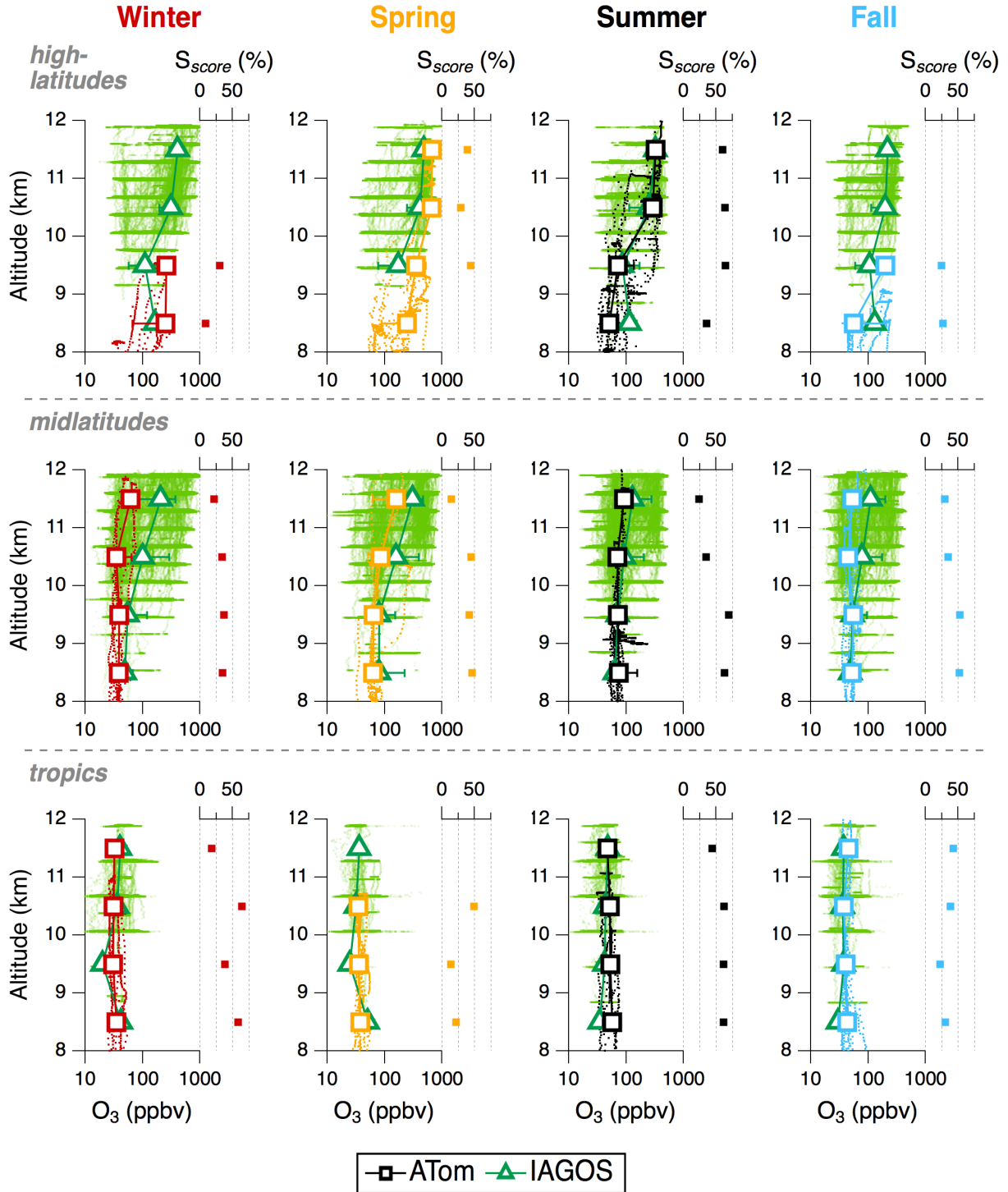


**Figure 7** Seasonal comparison of 1 km-binned ATom (colored squares) median  $O_3$  with IAGOS (green triangles) in the northern Atlantic UTLS. Markers indicate the median and the bars are the 25<sup>th</sup> and 75<sup>th</sup> percentiles. The three different rows indicate the latitudinal bands. The four columns

indicate the seasons. The green dots show every O<sub>3</sub> data point measured by IAGOS flights for the timeframe indicated in Table S1.

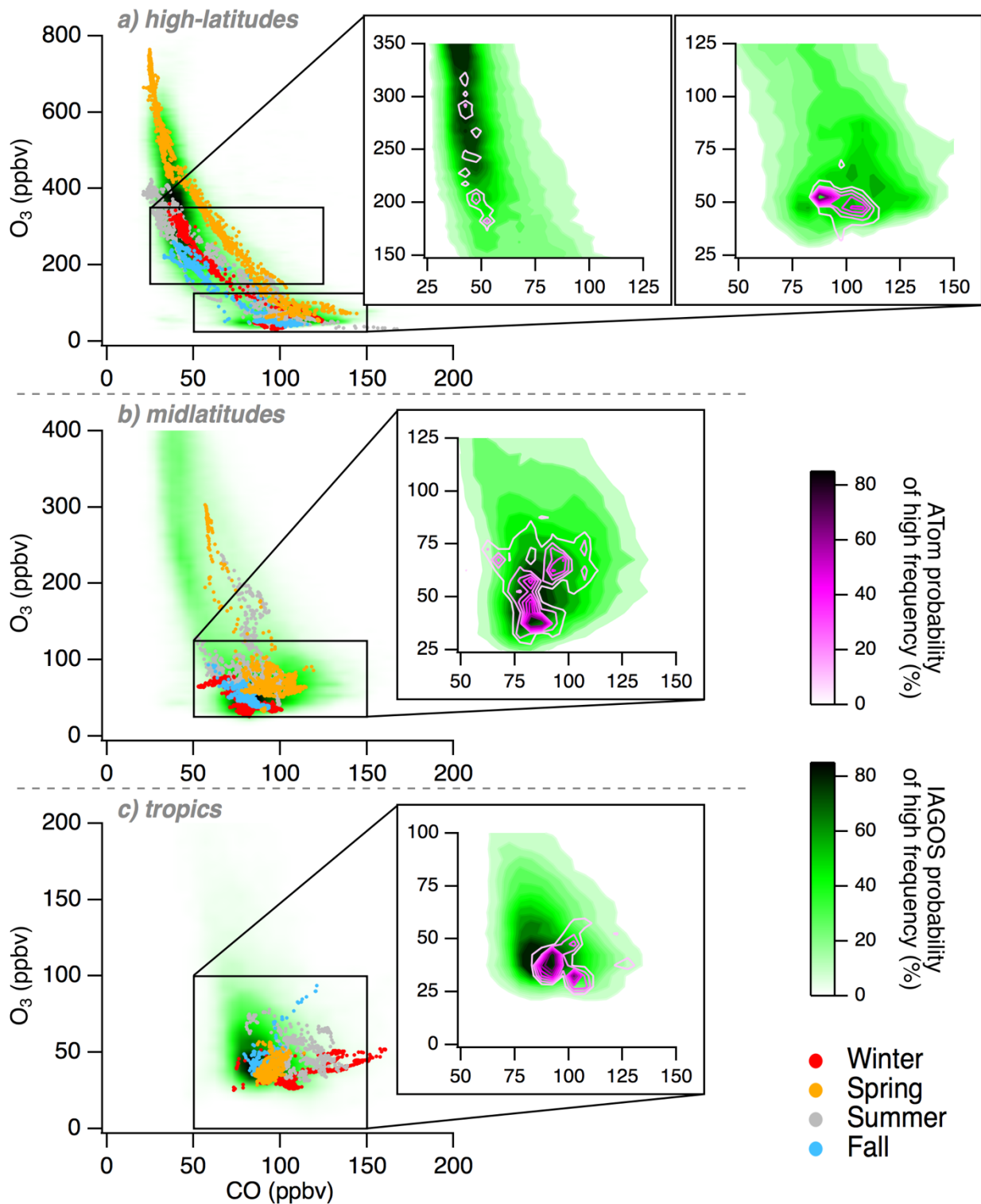


**Figure 8** IAGOS and ATom seasonal O<sub>3</sub> vs. CO scatterplots, with insets showing the most frequent O<sub>3</sub> values measured during IAGOS and ATom. ATom seasonal deployments are



colored according to the legend. The frequency gradient of O<sub>3</sub> counts is illustrated by the color scales (green for IAGOS, magenta for ATom). ATom measurements have been combined for the frequency gradients shown in the insets. The probability of high frequency refers to the probability of finding frequently measured O<sub>3</sub> values within the contour boundaries

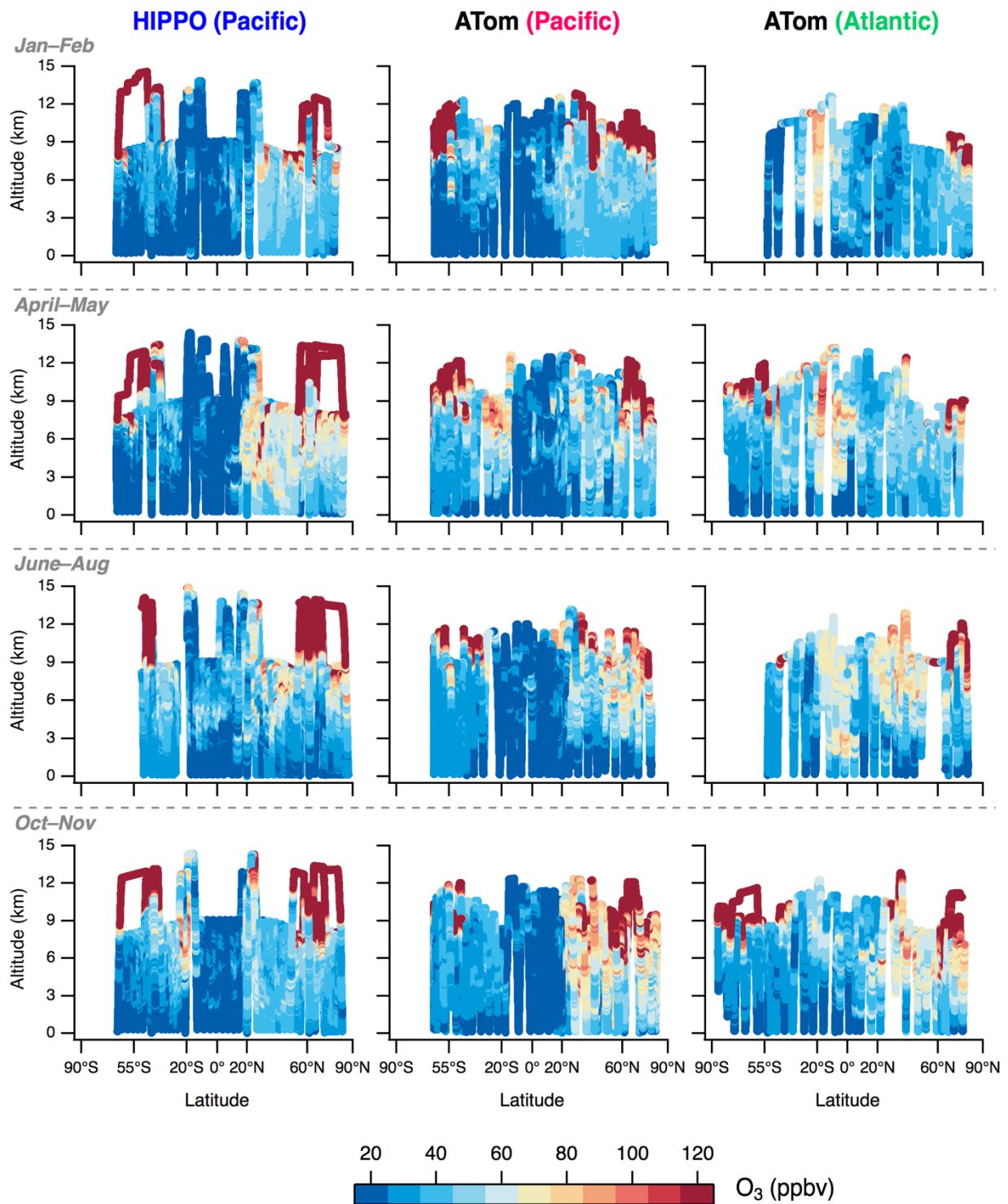


**Figure 9** Global-scale distribution of tropospheric  $O_3$  for each ATom and HIPPO seasonal deployment. The rows separate the seasonal deployments, while the columns indicate the mission and the ocean basin. The  $O_3$  color-scale ranges from 20 to 120 ppbv, and all values outside of this

range are shown with the same extremum color (red for values  $> 120$  ppbv, blue for values  $< 20$  ppbv). HIPPO deployments in June and August were combined together.

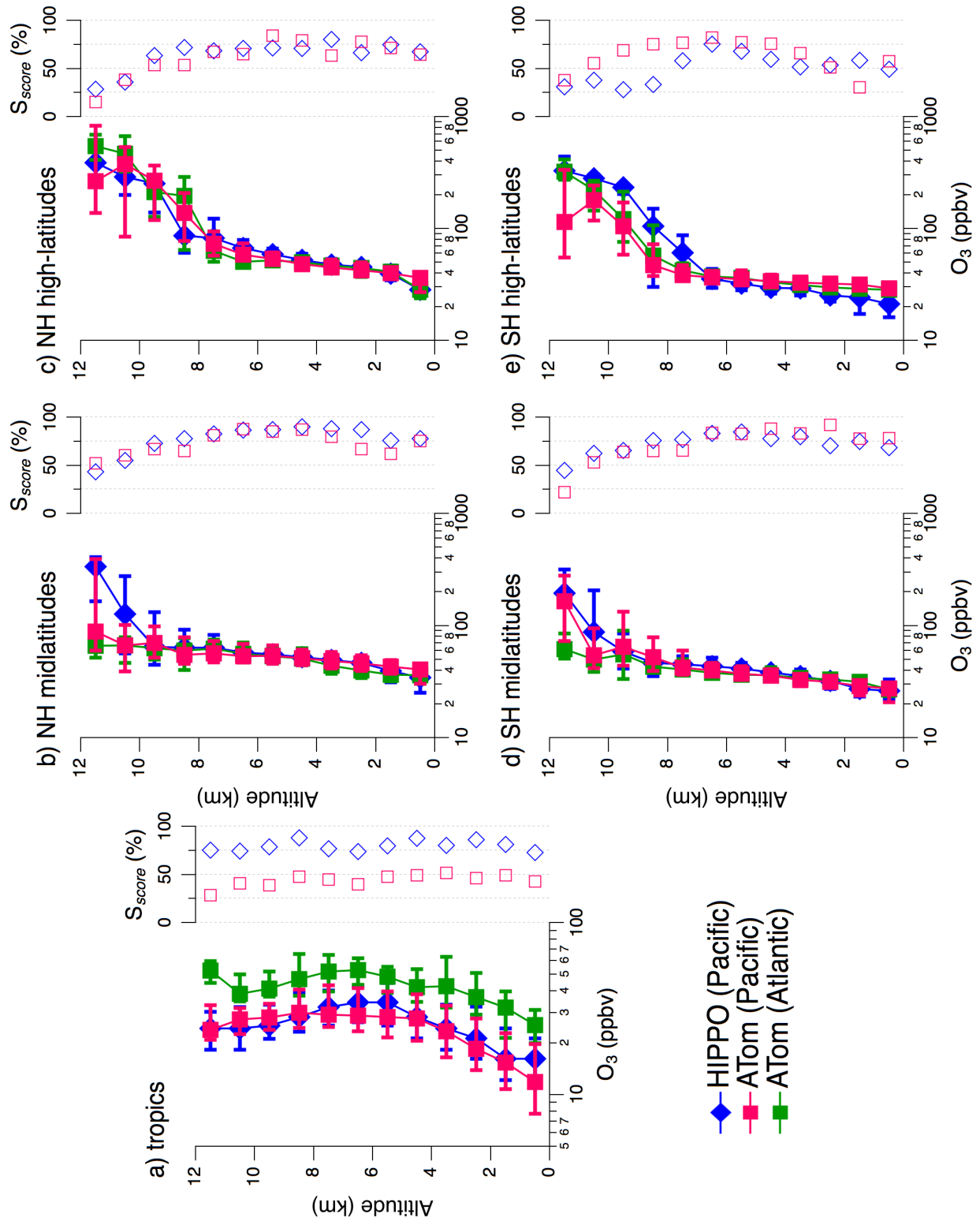


**Figure 10** Vertically-resolved  $O_3$  distributions from 0–12 km are plotted for the Atlantic (ATom in green) and for the Pacific (ATom in pink, HIPPO in blue). The five broad latitude regions correspond to the data parsing illustrated by Fig. 1. Markers indicate median  $O_3$ , and bars are the

25<sup>th</sup> and 75<sup>th</sup> percentiles, per 1 km altitude bin. Note the log scale on the x-axis.  $S_{score}$  values resulting from the comparison of HIPPO and ATom Pacific distributions are shown with blue diamonds, and from the comparison of ATom Atlantic and Pacific distributions with pink squares.

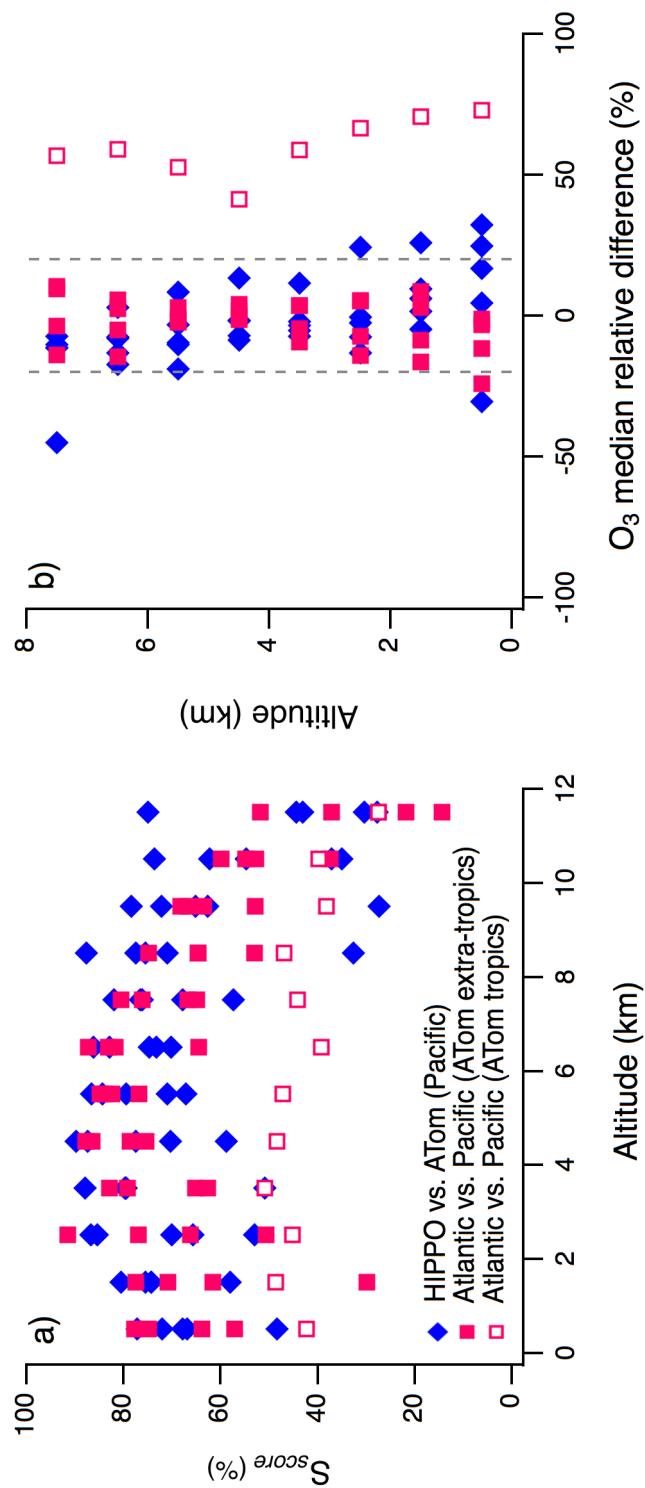


**Figure 11** All  $S_{score}$  values from Fig. 10 are shown in panel a) and plotted against altitude. The HIPPO and ATom comparison in the Pacific basin is shown with blue diamonds, and a comparison of the Atlantic and Pacific basins during ATom is shown with filled pink squares for the extra-

tropics and open pink squares for the tropics. The relative difference of median O<sub>3</sub> from 0 to 8 km given in Fig. 10 is shown in panel b), with the same color and marker code as in panel a). The dotted grey lines indicate a relative difference of 20 %.

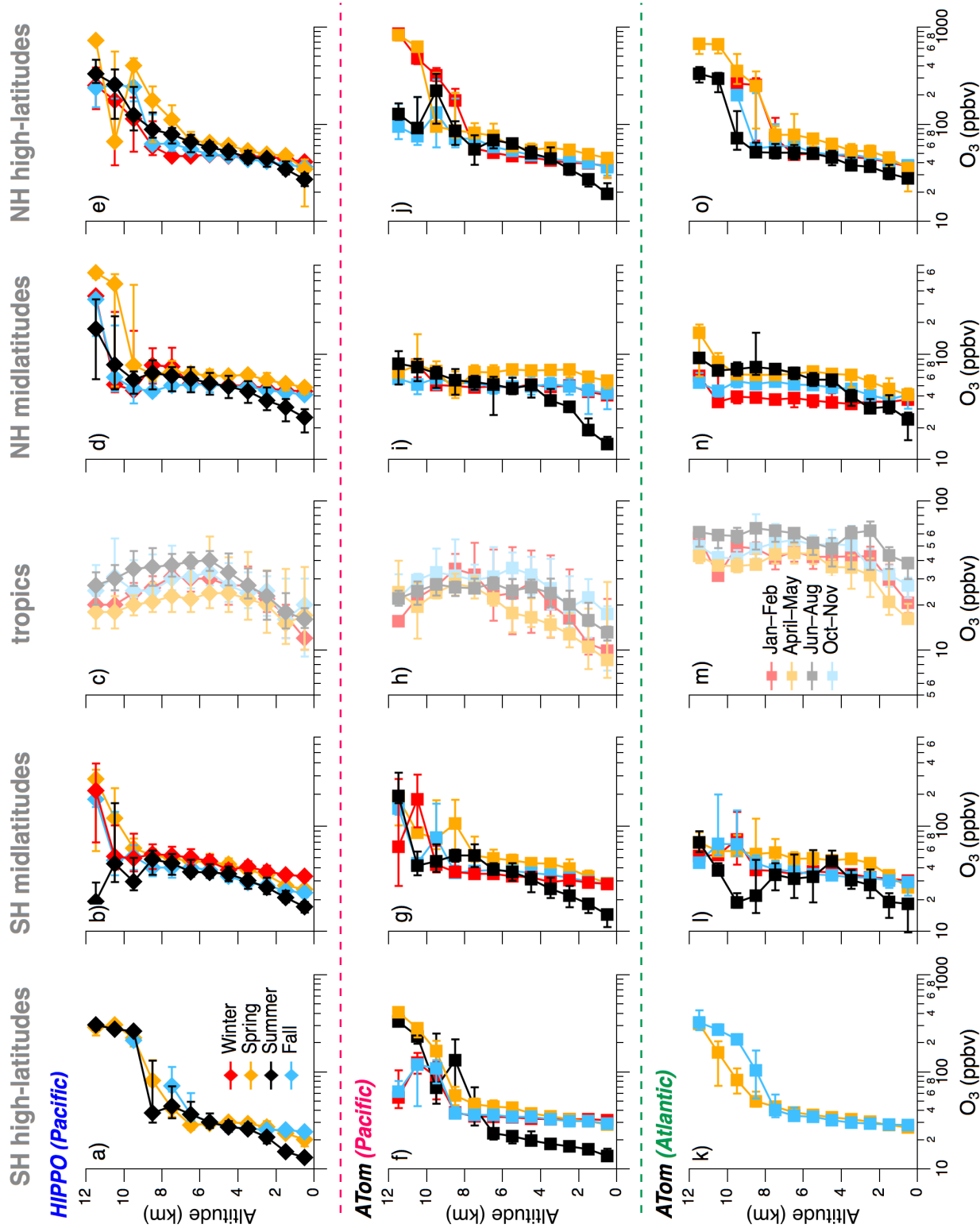


**Figure 12** Seasonal variability of regional  $O_3$  distribution in the Pacific (HIPPO in the first and ATom in the second row) and in the Atlantic (ATom in the third row). The colors designate the



local seasons with red as winter, gold as spring, black as summer, and blue as fall (corresponding months are indicated for the tropics, with lighter colors). The markers and associated bars correspond to the median, 25<sup>th</sup> and 75<sup>th</sup> percentiles, respectively, of O<sub>3</sub> distribution in every 1 km altitude bin. Note the logarithmic scale on the x-axes in all panels, and the changing scale with latitudinal bin.

**Figure 13** O<sub>3</sub> vs. CO plots using combined ATom and HIPPO data. Each panel denotes a different latitudinal band in each basin. Seasonal deployments are colored according to the legend. Note the logarithmic scale on the y-axis in all panels, and the changing scale with latitudinal bin

